INTERNATIONAL JOURNAL FOR NUMERICAL METHODS IN FLUIDS
Int. J. Numer. Meth. Fluids 2006; **51**:77–115
Published online 15 November 2005 in Wiley InterScience (www.interscience.wiley.com). DOI: 10.1002/fld.1119

On steady state computation of turbulent flows using k–ε models approximated by the time splitting method

Tao Du[1,2], Zi-Niu Wu[3,*,†] and Bing Wang[3]

[1]*Department of Engineering Mechanics, Tsinghua University, Beijing 100084, People's Republic of China*
[2]*Research & Development Center, CALT, Beijing 100076, People's Republic of China*
[3]*Department of Engineering Mechanics, Tsinghua University, Beijing 100084, People's Republic of China*

SUMMARY

The time splitting method is frequently used in numerical integration of flow equations with source terms since it allows almost independent programming for the source part. In this paper we will consider the question of convergence to steady state of the time splitting method applied to k–ε turbulence models. This analysis is derived from a properly defined scalar study and is carried out with success for the coupled k–ε equations. It is found that the time splitting method does not allow convergence to steady state for any choice of finite values of the time step. Numerical experiments for some typical turbulent compressible flow problems support the fact that the time splitting method is always nonconvergent, while its nonsplitting counterpart is convergent. Copyright © 2005 John Wiley & Sons, Ltd.

KEY WORDS: k–ε model; time splitting method; convergence to steady state

1. INTRODUCTION

Turbulence models involve nonlinear source terms. Numerous effects have been made to compute turbulent flows with such models [1–8]. The split method for treating problems with source terms has been presented in detail in Chapter 15 of Reference [9]. Kruzkov [10] proved the existence and uniqueness of the solution for the scalar conservation laws with source terms. Monthé [11] proved that the numerical solution of the splitting method converges towards the entropy solution in the scalar case. Conservation laws with source terms often have steady state solutions. Tang and Teng [12] proved this method always converges to the unique weak solution satisfying the entropy condition when computing discontinuous solutions of nonhomogeneous scalar conservation laws. However, it is well known that the time splitting method has difficulty in preserving the steady states. The so-called well-balanced

*Correspondence to: Z.-N. Wu, Department of Engineering Mechanics, Tsinghua University, Beijing 100084, People's Republic of China.
†E-mail: ziniuwu@tsinghua.edu.cn

Received 3 August 2004
Accepted 5 September 2005

schemes are introduced to capture the steady state solution of hyperbolic systems with source terms [13–15].

Splitting methods have been proposed for more general problems other than those with source terms [16, 17]. For example, in some large-scale engineering problems, operator splitting may be the only known practical way of carrying out time integration. In the area of geometric integration, such splitting methods are frequently used to obtain structure-preserving algorithms [18, 19]. Splitting is used in different ways, sometimes one applies splitting to the space dimensions, like in the original work of Strang [16]. Another much used possibility is to split according to some physical phenomenon, for instance, by splitting linear stiff diffusion terms and nonlinear convection terms and integrating each of them separately [20].

In this paper, we will investigate whether the time splitting method allows convergence to a (numerical) steady state for the important k–ε model suitable for describing engineering turbulent flows. Possibly, the calculation, starting with some initial state, yields a solution which oscillates in time, no matter how long we perform the integration. In this case, we also say that the calculation does not converge to zero machine.

We will first build a suitable method for the analysis of the numerical nonconvergence. There seems to be no efficient way but to first gain insight from a scalar analysis and then make an extension to the case of k–ε model.

We will first consider a scalar equation with linear, quadratic, cubic and n-order source terms. A method to give necessary condition of convergence to a numerical steady state will be built. We will also derive expressions for the steady state errors. Precisely, we will estimate the steady state error in terms of a stiffness parameter. The steady state error analysis will be extended to the k–ε model for turbulent flow computations. The result shows the splitting method will lead to nonconvergence for k–ε turbulence model equations, no matter how we diminish the time step.

The rest of the paper will be organized as follows. In Section 2 we briefly outline the time splitting method and build a method to estimate the steady state error. In Section 3, we analyse steady state errors for various scalar equations and present numerical experiments to support the validity of the theory. In Section 4, the analysis is extended to the two equation turbulence model. Numerical experiments will be presented in Section 5. Concluding remarks will be stated in Section 6.

2. TIME SPLITTING METHOD, CONVERGENCE AND STEADY STATE ERROR

2.1. Time splitting method

Consider the conservation law

$$U_t = P(\partial)U + S(U) \tag{1}$$

where $P(\partial)$ is the advection–diffusion operator and $S(U)$ is the source term.

Equation (1) is solved by a time splitting method, in which one alternates at each time iteration between solving the homogeneous conservation law (PDE step)

$$U_t = P(\partial)U \tag{2}$$

and the ordinary differential equation (ODE step)

$$U_t = S(U) \tag{3}$$

The exact steady state solution U, also called state equilibrium, satisfies

$$P(\partial)U + S(U) = 0 \tag{4}$$

which means that the source term and the homogeneous term balance each other, as expected for any steady problem.

Before proceeding further, we must emphasize that we are not dealing with nonconvergence due to spatial discretization. But in performing numerical computations in subsequent sections, we have to use spatial discretization for the PDE part. In that case, the steady state solution is the solution of the spatially discrete counterpart of (4). Hence, the analysis is performed just for the semidiscrete case (namely, discrete in time), but once we perform numerical computation the comparison is done for the fully discrete case. We have to discard the complexity using this simplification as one usually does, but fortunately this leads to useful results.

The approach we adopt to analyse the steady state errors is as follows. First, we assume that a steady state satisfying (4) exists. Then, we apply the time splitting method to this steady state solution. If the numerical increment remains to be zero or small enough, then this numerical scheme preserves this steady state. If this increment is large, then it means that a steady state can never be reached, and this increment can be interpreted as the steady state error of the numerical method (not to confuse with the error in steady state, which means errors in steady state due to spatial discretization).

Let U^0 be a solution satisfying the steady state equation (4) (or its spatially discrete counterpart, but in the subsequent analysis we no longer make this distinction).

Now, consider the numerical solution. The homogenous part will be approximated by the first-order Euler method in time. There is no need to know the details of the spatial discretization method for the PDE step. The ODE step will be approximated by an implicit method. In the next section we will also consider explicit numerical method and pure analytical method for the source term.

First, consider the numerical discretization of the homogeneous part

$$\bar{U}^1 = U^0 + \Delta t P(\partial) U^0$$

which, by using (4), can be written as

$$\bar{U}^1 = U^0 - \Delta t S(U^0) \tag{5}$$

This gives an intermediate solution $\bar{U}^1$ to be used as initial condition of the ODE step (3), whose numerical counterpart using implicit treatment reads

$$U^1 = \bar{U}^1 + \frac{\Delta t S(\bar{U}^1)}{\left(1 - \left.\dfrac{\partial S}{\partial U}\right|_{\bar{U}^1} \Delta t\right)} \tag{6}$$

where U^1 is the solution after an entire step and Δt is the time step.

2.2. Method to estimate the steady-state error

For convenience, we make the following definition.

Definition 1
The steady state error for the time splitting method is defined by

$$\delta U = U^1 - U^0 \tag{7}$$

or equivalently

$$R = \frac{U^1 - U^0}{U^0 - \zeta} \tag{8}$$

where ζ is the *stable equilibrium*, which is the solution for the equation $S(U) = 0$. For the time splitting method to preserve a steady state solution, we require R or δU to be small enough. Now we will estimate the steady state error δU or R.

Proposition 2
For the time splitting method, the steady state error is given by

$$\delta U = \frac{\Delta t \left[-\frac{(\Delta t S(U^0))^2}{2} \left.\frac{\partial^2 S}{\partial U^2}\right|_{U_0} + \frac{(\Delta t S(U^0))^3}{3} \left.\frac{\partial^3 S}{\partial U^3}\right|_{U_0} + \cdots \right]}{\left[1 - \left(\left.\frac{\partial S}{\partial U}\right|_{U_0} - \Delta t S(U^0) \left.\frac{\partial^2 S}{\partial U^2}\right|_{U_0} + \frac{(\Delta t S(U^0))^2}{2} \left.\frac{\partial^3 S}{\partial U^3}\right|_{U_0} + \cdots \right) \Delta t \right]} \tag{9}$$

Proof
Combining (5) and (6) yields

$$\begin{aligned} U^1 - U^0 &= \frac{\Delta t S(\bar{U}^1)}{\left(1 - \left.\frac{\partial S}{\partial U}\right|_{\bar{U}^1} \Delta t \right)} - \Delta t S(U^0) \\ &= \frac{\Delta t S\left(U^0 - \Delta t S(U^0)\right)}{\left(1 - \left.\frac{\partial S}{\partial U}\right|_{U^0 - \Delta t S(U^0)} \Delta t \right)} - \Delta t S(U^0) \end{aligned} \tag{10}$$

By expanding the two terms $S(U^0 - \Delta t S(U^0))$ and $\partial S/\partial U\,|_{U^0 - \Delta t S(U^0)}$ as

$$\begin{aligned} &S(U^0 - \Delta t S(U^0)) \\ &\quad = S(U^0) - \Delta t S(U^0) \left.\frac{\partial S}{\partial U}\right|_{U_0} + \frac{(\Delta t S(U^0))^2}{2} \left.\frac{\partial^2 S}{\partial U^2}\right|_{U_0} - \frac{(\Delta t S(U^0))^3}{3!} \left.\frac{\partial^3 S}{\partial U^3}\right|_{U_0} \\ &\qquad + O((\Delta t S(U^0))^4) \end{aligned}$$

and

$$\left.\frac{\partial S}{\partial U}\right|_{U_0-\Delta tS(U^0)} = \left.\frac{\partial S}{\partial U}\right|_{U_0} - \Delta tS(U^0)\left.\frac{\partial^2 S}{\partial U^2}\right|_{U_0} + \frac{(\Delta tS(U^0))^2}{2}\left.\frac{\partial^3 S}{\partial U^3}\right|_{U_0} + O((\Delta tS(U^0))^3)$$

we obtain the final expression (9) from (10). □

One can also solve the ordinary differential equation (3) first and treat the homogeneous PDE part next, see Reference [11]. In this case, we have

$$\bar{U}^1 = U^0 - \frac{\Delta tS(U^0)}{\left(1 + \left.\frac{\partial S}{\partial U}\right|_{U^0}\Delta t\right)} \tag{11}$$

$$U^1 = \bar{U}^1 + \Delta tS(\bar{U}^1) \tag{12}$$

Using (11) and (12) we obtain

$$\begin{aligned}\delta U = U^1 - U^0 &= \Delta tS(\bar{U}^1) - \frac{\Delta tS(U^0)}{\left(1 + \left.\frac{\partial S}{\partial U}\right|_{U^0}\Delta t\right)} \\ &= \Delta tS\left[U^0 - \frac{\Delta tS(U^0)}{\left(1 + \left.\frac{\partial S}{\partial U}\right|_{U^0}\Delta t\right)}\right] - \frac{\Delta tS(U^0)}{\left(1 + \left.\frac{\partial S}{\partial U}\right|_{U^0}\Delta t\right)}\end{aligned} \tag{13}$$

which, after using Taylor expansion, yields

$$\delta U = \Delta t\left[S(U^0) - \left.\frac{\partial S}{\partial U}\right|_{U^0}\frac{\Delta tS(U^0)}{\left(1 + \left.\frac{\partial S}{\partial U}\right|_{U^0}\Delta t\right)} + \frac{1}{2}\left.\frac{\partial^2 S}{\partial U^2}\right|_{U^0}\left\{\frac{\Delta tS(U^0)}{\left(1 + \left.\frac{\partial S}{\partial U}\right|_{U^0}\Delta t\right)}\right\}^2\right]$$
$$-\frac{\Delta tS(U^0)}{\left(1 + \left.\frac{\partial S}{\partial U}\right|_{U^0}\Delta t\right)}$$

$$= \Delta t S(U^0) - \left(\Delta t \left.\frac{\partial S}{\partial U}\right|_{U^0} + 1\right) \frac{\Delta t S(U^0)}{\left(1 + \left.\frac{\partial S}{\partial U}\right|_{U^0} \Delta t\right)} + \frac{\Delta t}{2} \left.\frac{\partial^2 S}{\partial U^2}\right|_{U^0} \left\{ \frac{\Delta t S(U^0)}{\left(1 + \left.\frac{\partial S}{\partial U}\right|_{U^0} \Delta t\right)} \right\}^2 + O((\Delta t S(U^0))^3)$$

$$\doteq \frac{\Delta t}{2} \left.\frac{\partial^2 S}{\partial U^2}\right|_{U^0} \left\{ \frac{\Delta t S(U^0)}{\left(1 + \left.\frac{\partial S}{\partial U}\right|_{U^0} \Delta t\right)} \right\}^2 \tag{14}$$

The steady state error (8) can also be estimated by using (14) for any specific source term $S(U)$.

3. STEADY STATE ERRORS FOR SOME KINDS OF SOURCE TERMS AND NUMERICAL EXPERIMENTS

In this section we consider power-function-type source term.

3.1. General high-order nonlinear source term

In this part, we consider the general source term in the form

$$S(U) = -c(U - s(x))^n, \quad (n \geqslant 2 \text{ and } n \in N)$$

Proposition 3
For the general source term $s = -c(U - s(x))^n, (n \geqslant 2)$, c is a constant, the steady state error ratio is given by

$$R(Y) = \frac{\frac{1}{2}n(n-1)Y^3 + \frac{1}{3}n(n-1)(n-2)Y^4}{1 + nY + n(n-1)Y^2 + \frac{1}{2}n(n-1)(n-2)Y^3} \tag{15}$$

where

$$Y = c\Delta t(U^0 - s(x))^{n-1} \tag{16}$$

is the stiffness parameter.

Proof
Substitute $S(U) = -c(U - s(x))^n$ into (9), we obtain

$$\delta U = U^1 - U^0 = \frac{A + B}{1 - \Delta t[C - D]}$$

with

$$A = \tfrac{1}{2}n(n-1)(c\Delta t)^3(U^0 - s(x))^{3n-2}$$

$$B = \tfrac{1}{3}n(n-1)(n-2)(c\Delta t)^4(U^0 - s(x))^{4n-3}$$

$$C = -nc(U - s(x))^{n-1} - n(n-1)c^2\Delta t(U^0 - s(x))^{2n-2}$$

$$D = \tfrac{1}{2}n(n-1)(n-2)c^2(\Delta t)^3(U^0 - s(x))^{3n-3}$$

Then, we have

$$R = \frac{\delta U}{U^0 - s(x)}$$

$$= \frac{-\frac{1}{2}n(n-1)Y^3 + \frac{1}{3}n(n-1)(n-2)Y^4}{1 + nY + n(n-1)Y^2 + \frac{1}{2}n(n-1)(n-2)Y^3}$$

where $Y = (c\Delta t)(U^0 - s(x))^{n-1}$. □

3.2. Linear source term

In the case of a linear source term, $S(U)$ is defined by

$$S(U) = -cU \tag{17}$$

Using (9) for the linear source term (17), we find that the steady state error is zero, i.e. the time splitting method preserves steady states for a linear source term. In other words, *the time splitting method allows for convergence to a steady state for a linear source term.*

Now we perform numerical calculations just for the following scalar equation:

$$\frac{\partial U}{\partial t} + \frac{\partial f(U)}{\partial x} = -c(U - s(x)) \tag{18}$$

Here, $f(U)$ is flux function. The advection term is discretized by first-order upwind scheme (using other kinds of stable schemes does not affect the conclusions).

Example 1

The problem is defined by

$$c = 1, \quad f(U) = 5U, \quad s(x) = \begin{cases} x^2/1000 & 0 \leqslant x \leqslant 50 \\ (x-100)^2/1000 & 50 \leqslant x \leqslant 100 \end{cases}$$

$$U(x,0) = 3 \quad \text{for } x > 0, \quad U(0,t) = 0 \quad \text{for } t > 0$$

The time step is $\Delta t = 0.04$, the space grid scale is $\Delta h = 0.2$. The CFL (Courant, Friedrichs, Lewy) number is 1 so that the method is stable in the sense of von Neumann. The implicit treatment for the source term in the second step guarantees unconditional stability of the

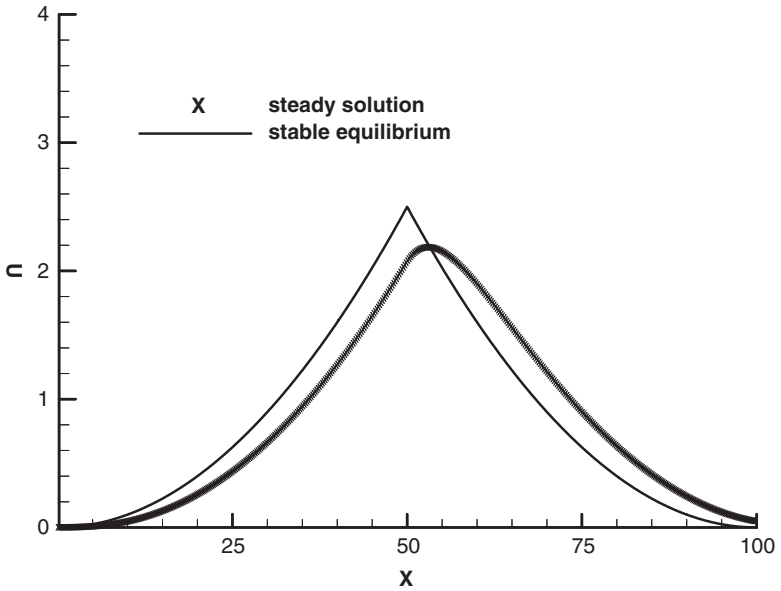

Figure 1. The converged numerical result for example 1. Note that the difference between the numerical steady state solution and the steady state equilibrium (steady state solution of the exact equation) is due to spatial discretization.

source-term treatment. The calculation converges to a steady state close to the stable equilibrium. The stable equilibrium is the solution for the source equation $S(U)=0$ (see Reference [21]). The steady state (numerical) solution is displayed in Figure 1. We also displayed the stable equilibrium of the exact equation. Note that the discrepancy between the numerical steady state solution and the exact steady state solution is due to spatial discretization, not due to convergence in time.

The convergence evolution based on the residual is shown in Figure 2.

Example 2
The problem is defined by

$$c=1, \quad f(U)=U^2, \quad s(x)=\begin{cases} x^2/1000 & 0 \leqslant x \leqslant 50 \\ (x-100)^2/1000 & 50 \leqslant x \leqslant 100 \end{cases}$$

$$U(x,0)=3 \quad \text{for } x>0, \quad U(0,t)=0 \quad \text{for } t>0$$

The time step is $\Delta t=0.03$, which meets the CFL condition requirement, and the space grid scale is $\Delta h=0.2$. Similarly as in the previous case, the calculation converges to a steady state without difficulty. The smooth convergent steady solution is shown in Figure 3, which compares well with the stable equilibrium. The convergence evolution of maximum residual is shown in Figure 4.

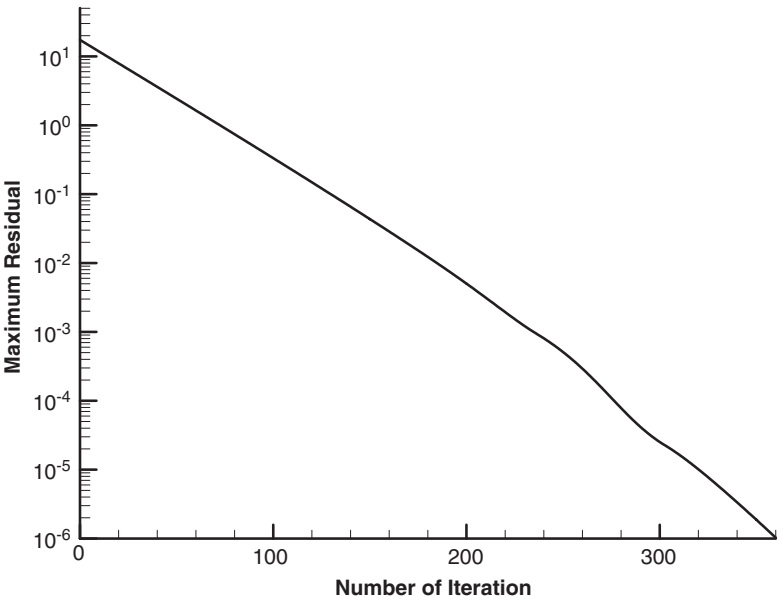

Figure 2. Convergence history for example 1.

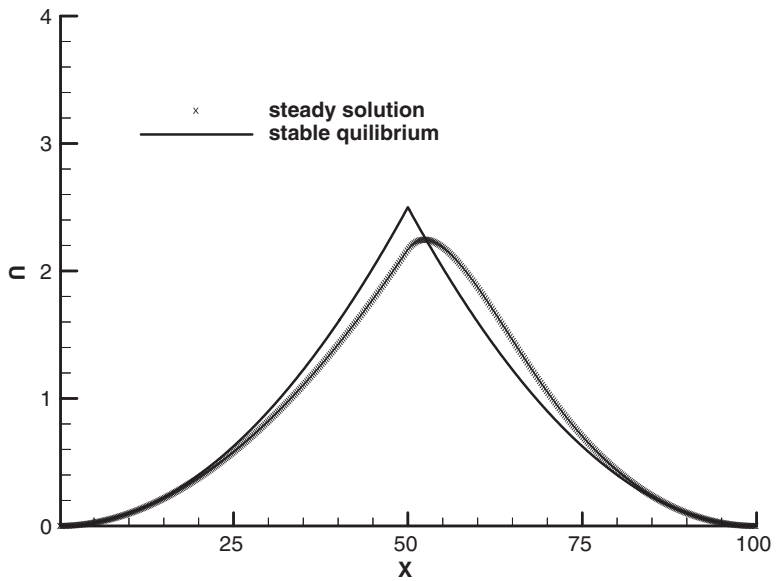

Figure 3. The numerical result for example 2. Note that the difference between the numerical steady state solution and the steady state equilibrium (steady state solution of the exact equation) is due to spatial discretization.

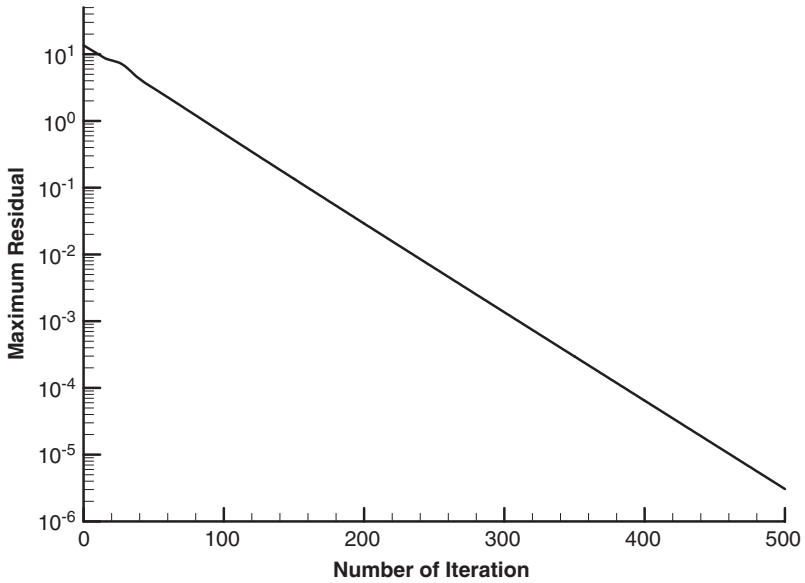

Figure 4. Convergence history for example 2.

3.3. Second-order nonlinear source term

In the case of a second-order source term, $S(U)$ is defined by

$$S(U) = -c(U - s(x))^2 \tag{19}$$

According to formula (15), for the source term (19), the steady state error is given by

$$R(Y) = \frac{Y^3}{1 + 2Y + 2Y^2} \tag{20}$$

where

$$Y = c\Delta t(U^0 - s(x)) \tag{21}$$

is the stiffness parameter.

The steady state error $R = R(Y)$ is displayed in Figure 5. It is clear that the steady state error R increases monotonously with Y. The error R is of order 1 when Y is larger than 1. Hence, an acceptable steady state cannot be reached unless Y is very small.

Example 3

Consider the scalar equation

$$\frac{\partial U}{\partial t} + a\frac{\partial U}{\partial x} = -c(U - s(x))^2 \tag{22}$$

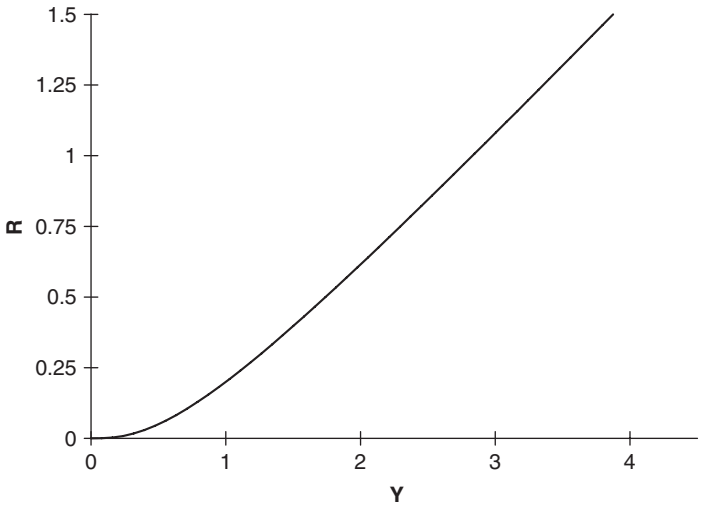

Figure 5. The steady state error $R = R(Y)$ as a function of the stiffness parameter $Y = \Delta t U^0$.

Discretize Equation (22) with the Yee–Roe–Davis symmetric second-order TVD scheme for the space terms [22]. The following parameters are considered:

$$a = 0.05, \quad c = 1, \quad s(x) = 20 \exp(-x^2/250)$$

The initial condition and boundary condition are given by

$$U(x, 0) = 25 \quad \text{for } x > 0, \quad U(0, t) = 20 \quad \text{for } t > 0$$

The spatial mesh width is $\Delta h = 0.2$. In order to meet $\text{CFL} = a(\Delta t/\Delta x) \leqslant 1$, the maximum allowable time step Δt is 4.0. We select $\Delta t = 3.0$ ($Y = 0.7$ estimated). The numerical solution does not converge to a steady state. Figure 6 displays the numerical results after a long time integration. We find that the nonconverged numerical solution is not smooth, while the exact solution is a smooth one. When we choose smaller time steps, say $\Delta t = 0.43$ and $\Delta t = 0.043$ (which corresponds to $Y = 0.1$ and $Y = 0.01$ estimated), the steady state errors are negligibly small, as can be shown in Figure 7. Figure 8 shows the convergence histories of the maximum residual for various time steps (or Y). When the steady state error is large, the calculation does not converge to zero machine. For $\Delta t = 3.0, 1.5, 1.0, 0.7$ and 0.043, the residual $\Delta U = (U_j^{n+1} - U_j^n)$ is compared with the theoretical prediction $R(Y)(U_j^n - s(x_j))$ in Figures 9–13, respectively. When time step is larger, the calculations do not converge. From these pictures, we can see that the theoretical estimation of the steady state error is close to the numerical residual. This means that the analytical method for the steady state error built in Section 2 is useful for the present purpose.

3.4. Third-order nonlinear source term

Now consider the third-order source term defined as

$$S(U) = -c(U - s(x))^3 \tag{23}$$

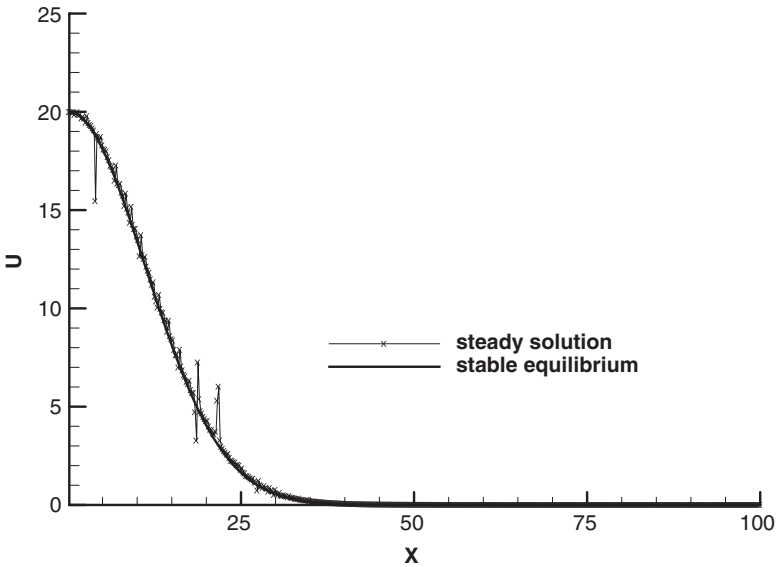

Figure 6. Long time solution U^0 in example 3. No steady state can be obtained for the numerical solution.

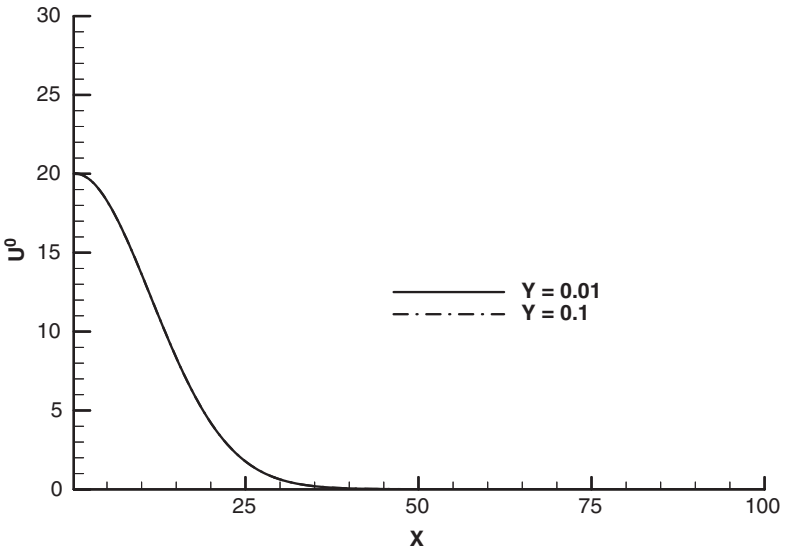

Figure 7. The steady solution U^0 in example 3: $Y = 0.1$ and $Y = 0.01$.

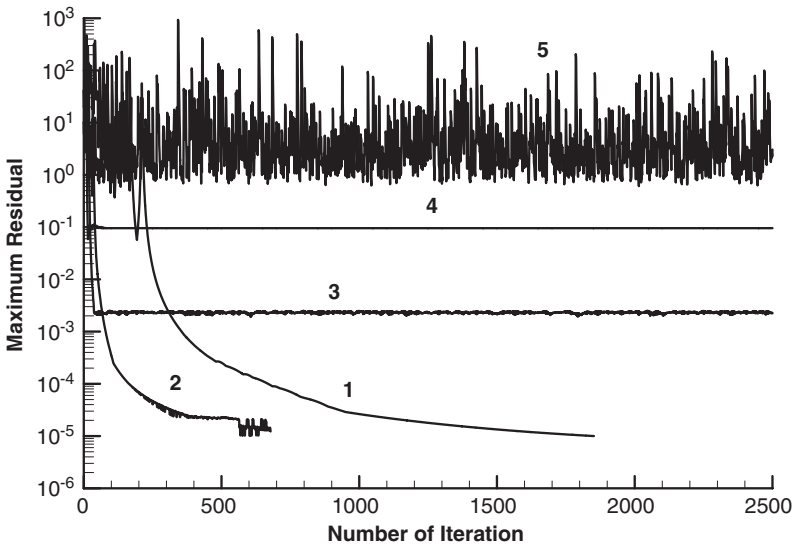

Figure 8. Convergence histories in terms of the maximal residual for example 3: $\Delta t = 0.043 (Y = 0.01)$, line 1; $\Delta t = 0.43 (Y = 0.1)$, line 2; $\Delta t = 1.0 (Y = 0.23)$, line 3; $\Delta t = 1.5 (Y = 0.35)$, line 4; $\Delta t = 3.0 (Y = 0.7)$, line 5.

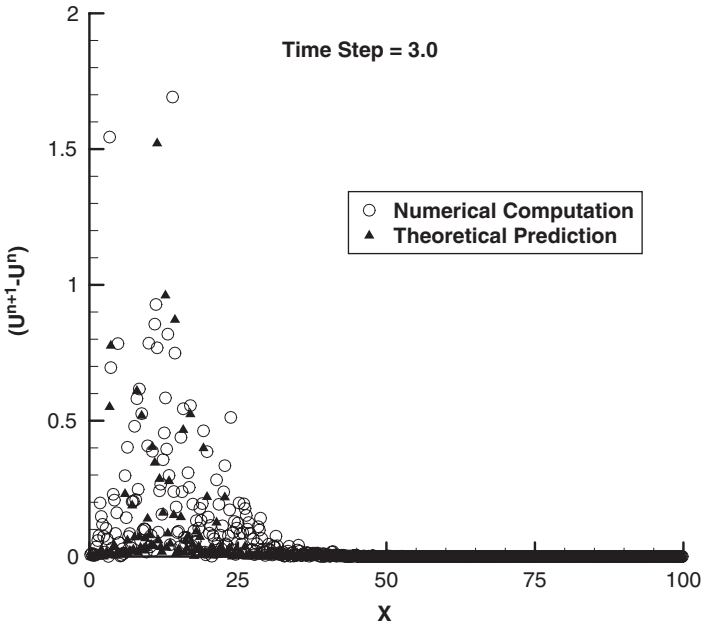

Figure 9. Comparison between the computed numerical residual ΔU and theoretical prediction with $\Delta t = 3.0$ in example 3.

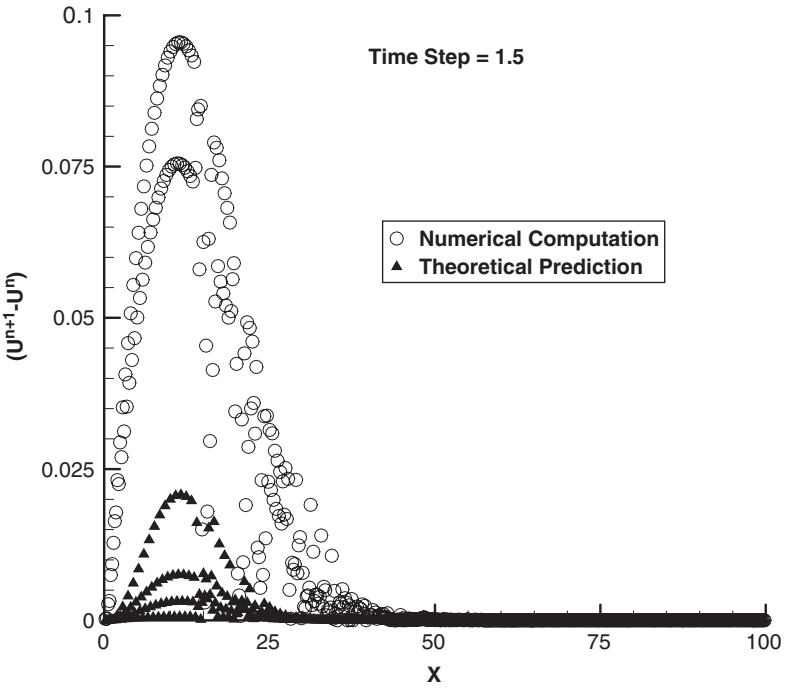

Figure 10. Comparison between the computed numerical residual ΔU and theoretical prediction with $\Delta t = 1.5$ in example 3.

According to (15), for the source term (23), the steady state error is given by

$$R = \frac{3Y^3 + 2Y^4}{1 + 3Y(1+Y)^2} \tag{24}$$

where

$$Y = c\Delta t(U^0 - s(x))^2 \tag{25}$$

is the stiffness parameter.

The steady state error (24) is plotted in Figure 14 as a function of Y. When Y is larger than 0.4, the absolute value of R increases rapidly with Y. Only when Y is much less than 0.4, the steady state error is small.

Example 4

Consider the scalar equation

$$\frac{\partial U}{\partial t} + a\frac{\partial U}{\partial x} = -c(U-1)^3 \tag{26}$$

$$U(x,0) = 2, \quad \text{for } x > 0, \quad U(0,t) = 2 \quad \text{for } t > 0 \tag{27}$$

where $a = 0.5$ and $c = 1.0$.

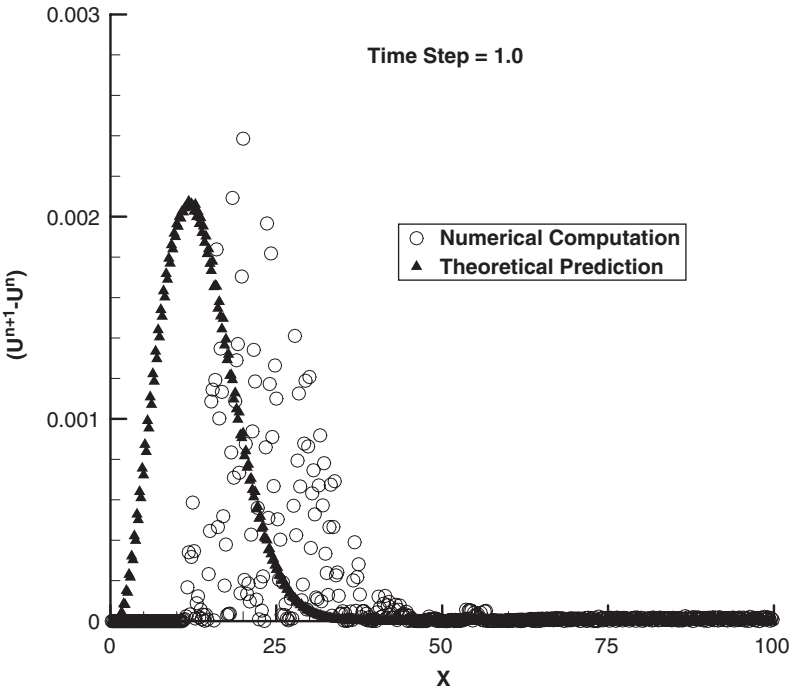

Figure 11. Comparison between the computed numerical residual ΔU and theoretical prediction with $\Delta t = 1.0$ in example 3.

For example 4, the stiffness parameter is $Y = c\Delta t(U^0 - 1)^2$, the steady state error is given by (24).

The steady state solution of this problem is given by

$$U = 1 + \frac{1}{\sqrt{2\frac{c}{a}x + 1}} \tag{28}$$

The spatial mesh width is $\Delta h = 1.0$ and the computational domain is $[0, 10]$. We select $\Delta t = 1.5$ (CFL $= 0.75$) and 0.5 (CFL $= 0.25$), which correspond to $Y = 1.5$ and $Y = 0.5$, respectively. The numerical solutions are shown in Figure 15. The solution with $\Delta t = 1.5$ does not converge to zero machine, as displayed in Figure 16.

3.5. Other kinds of schemes for the source term

In the previous analysis we have just considered an implicit scheme for the source term. Here, we just consider the source term $S(U) = -U^2$ and derive steady state errors for two other kinds of scheme.

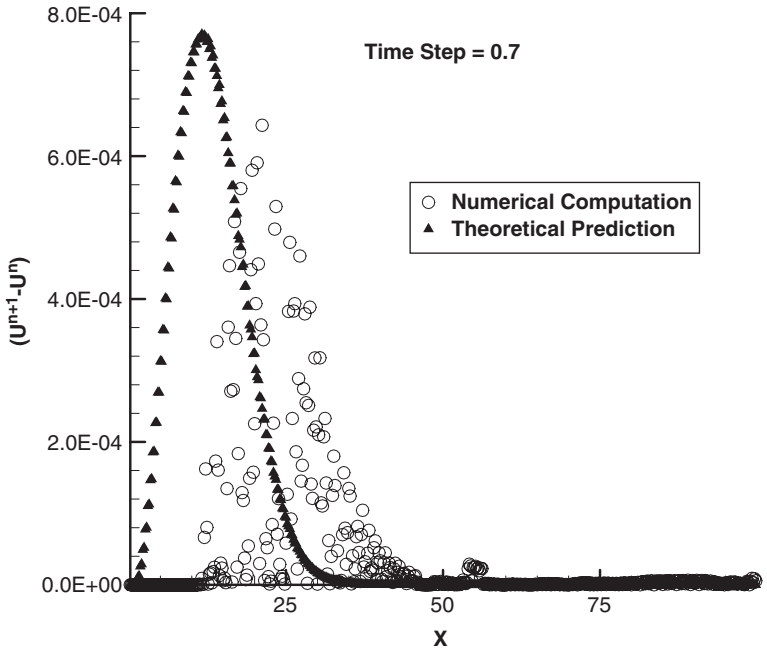

Figure 12. Comparison between the computed numerical residual ΔU and theoretical prediction with $\Delta t = 0.7$ in example 3.

(1) *Explicit scheme for the source term*. When we use an explicit scheme, say the first-order Euler scheme, for the source term, then the time splitting method can be expressed as

$$\bar{U}^1 = U^0 - \Delta t S(U^0) = U^0 + \Delta t U^{02} \tag{29}$$

$$U^1 = \bar{U}^1 + \Delta t S(\bar{U}^1) \tag{30}$$

and the steady state error is given by

$$R = \frac{U^1 - U^0}{U^0} = \frac{-2\Delta t^2 U^{03} - \Delta t^3 U^{04}}{U^0} = -2(\Delta t U^0)^2 - (\Delta t U^0)^3$$

$$= -2Y^2 - Y^3 \tag{31}$$

The steady state error R is plotted in Figure 17, which shows that the steady state error is very large for large values of Y.

(2) *Mixed analytical/numerical method* [1]. In this method, the ODE for the source term is integrated exactly, so that the entire scheme is defined by

$$\bar{U}^1 = U^0 - \Delta t S(U^0) = U^0 + \Delta t (U^0)^2 \tag{32}$$

$$U^1 = \frac{\bar{U}^1}{\bar{U}^1 \Delta t + 1} \tag{33}$$

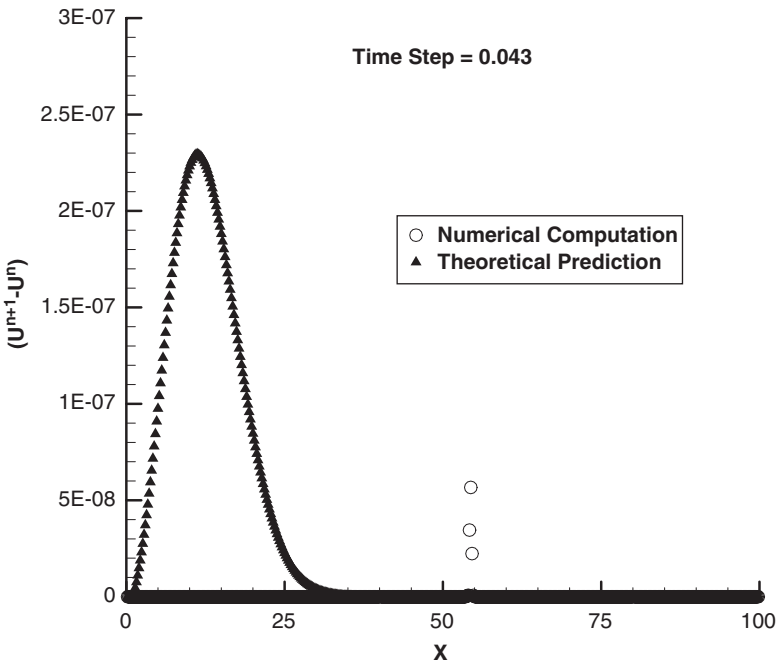

Figure 13. Comparison between the computed numerical residual ΔU and theoretical prediction with $\Delta t = 0.043$ in example 3.

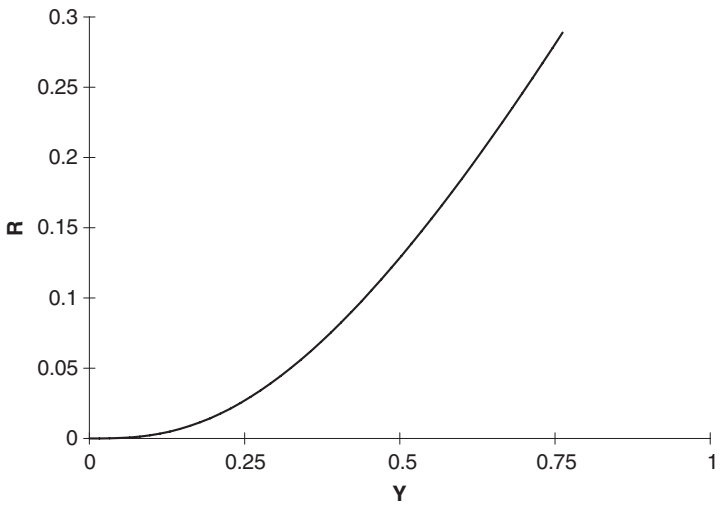

Figure 14. The steady state error function $R = R(Y)$ for $Y = \Delta t(U^0)^2$.

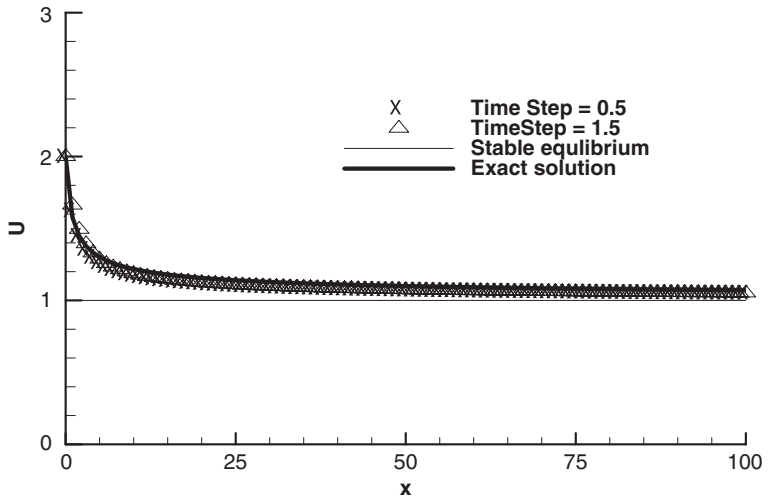

Figure 15. The steady solution U^0 in example 4: $\Delta t = 0.5$ and $\Delta t = 1.5$.

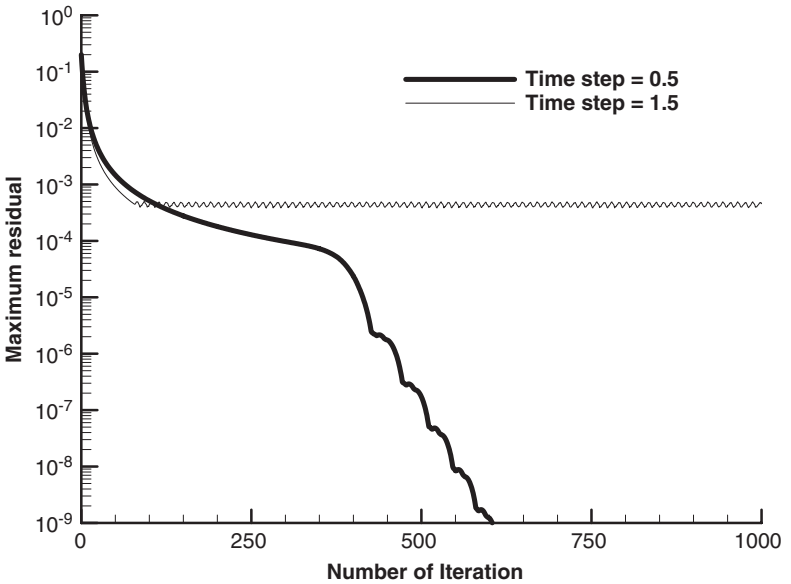

Figure 16. Convergence histories in terms of the maximal residual for example 4.

and the steady state error satisfies

$$R = \frac{U^1 - U^0}{U^0} = \frac{-\Delta t^2 (U^0)^3}{U^0(1 + \Delta t U^0 + \Delta t^2 (U^0)^2)} = \frac{-(\Delta t U^0)^2}{1 + (\Delta t U^0) + (\Delta t U^0)^2}$$

$$= \frac{-Y^2}{1 + Y + Y^2} \tag{34}$$

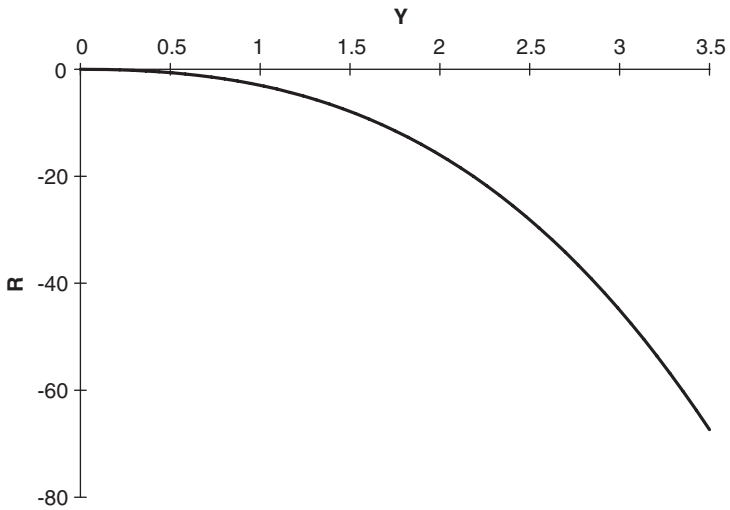

Figure 17. The steady state error R as a function of Y for the explicit treatment of the source term.

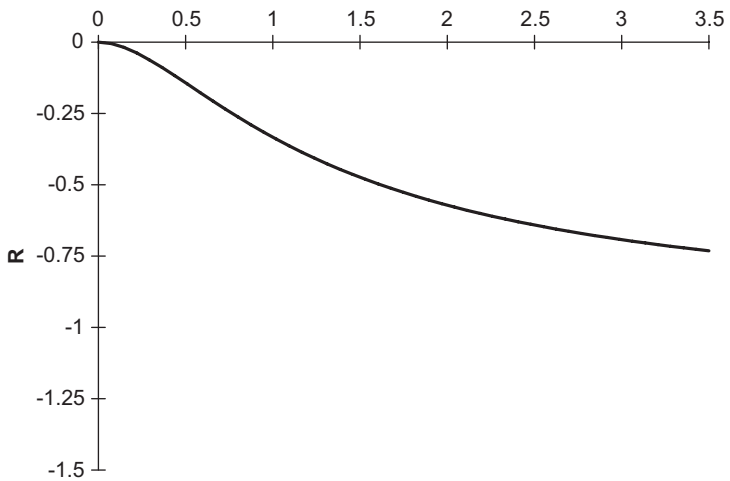

Figure 18. The steady state error R as a function of Y for the analytical treatment of the source term.

The steady state error R is plotted in Figure 18, which shows that the steady state error is very large for large values of Y.

Hence, the qualitative conclusions are almost independent of the scheme for the treatment of the source term.

4. STEADY STATE ERROR FOR THE STANDARD k–ε TURBULENT MODEL

4.1. The high-Reynolds number k–ε turbulence model

The standard k–ε turbulence model can be written as

$$\frac{\partial U^{\mathrm{T}}}{\partial t}+\frac{\partial F_c^{\mathrm{T}}}{\partial x}+\frac{\partial G_c^{\mathrm{T}}}{\partial y}=\frac{\partial F_v^{\mathrm{T}}}{\partial x}+\frac{\partial G_v^{\mathrm{T}}}{\partial y}+S \tag{35}$$

where U^{T}, F_c^{T}, and G_c^{T} are defined by

$$U^{\mathrm{T}}=\begin{pmatrix}\rho k\\ \rho\varepsilon\end{pmatrix}\quad F_c^{\mathrm{T}}=\begin{pmatrix}\rho uk\\ \rho u\varepsilon\end{pmatrix}\quad G_c^{T}=\begin{pmatrix}\rho vk\\ \rho v\varepsilon\end{pmatrix} \tag{36}$$

Here, k and ε denote the turbulent kinetic energy and turbulent dissipation rate. The diffusive fluxes F_v^{T} and G_v^{T} are given by

$$F_v^{\mathrm{T}}=\begin{bmatrix}\left(\mu+\dfrac{\mu_t}{\sigma_k}\right)\dfrac{\partial k}{\partial x}\\ \left(\mu+\dfrac{\mu_t}{\sigma_\varepsilon}\right)\dfrac{\partial \varepsilon}{\partial x}\end{bmatrix}\quad G_v^{\mathrm{T}}=\begin{bmatrix}\left(\mu+\dfrac{\mu_t}{\sigma_k}\right)\dfrac{\partial k}{\partial y}\\ \left(\mu+\dfrac{\mu_t}{\sigma_\varepsilon}\right)\dfrac{\partial \varepsilon}{\partial y}\end{bmatrix} \tag{37}$$

The source term S is given by

$$S=\begin{bmatrix}\mu_t P_k-\rho\varepsilon\\ C_{\varepsilon1}\mu_t\dfrac{\varepsilon}{k}P_k-C_{\varepsilon2}\dfrac{\rho\varepsilon^2}{k}\end{bmatrix} \tag{38}$$

where the production P_k is given by

$$P_k=\left(\frac{\partial U_i}{\partial x_k}-\frac{\partial U_k}{\partial x_i}\right)\frac{\partial U_i}{\partial x_k} \tag{39}$$

The eddy viscosity is calculated as

$$\mu_t=C_\mu\rho k^2/\varepsilon$$

where $C\mu$, $C_{\varepsilon1}$, $C_{\varepsilon2}$, σ_k and σ_ε are 0.09, 1.44, 1.9, 1.0 and 1.3, respectively.

4.2. Numerical method based on time splitting

The splitting method is divided into two steps:

(1) *Advection diffusion part*

$$\frac{\partial \bar{U}^{\mathrm{T}}}{\partial t}+\frac{\partial F_c^{\mathrm{T}}}{\partial x}+\frac{\partial G_c^{\mathrm{T}}}{\partial y}=\frac{\partial F_v^{\mathrm{T}}}{\partial x}+\frac{\partial G_v^{\mathrm{T}}}{\partial y},\quad t^n<t<t^{n+1} \tag{40}$$

$$\bar{U}^{\mathrm{T}}(t^n)=(U^{\mathrm{T}})^n \tag{41}$$

(2) *Source term part*

$$\frac{\mathrm{d}U^{\mathrm{T}}}{\mathrm{d}t} = S(U^{\mathrm{T}}), \quad t^n < t < t^{n+1}$$
$$U^{\mathrm{T}}(t^n) = \bar{U}^{\mathrm{T}}(t^{n+1}) \tag{42}$$

which could be integrated analytically [1–3] or numerically to obtain $U^{\mathrm{T}}(t^{n+1})$ to be used for the next iteration.

4.3. Steady state errors

In the source term (38), the production terms are always positive while the dissipation terms are always negative. For convenience, we rewrite the source term as

$$S = \begin{bmatrix} \mu_t P_k - \dfrac{C_\mu}{\mu_t}(\rho k)^2 \\ \\ C_{\varepsilon 1}(C_\mu \mu_t)^{1/2} P_k (\rho\varepsilon)^{1/2} - C_{\varepsilon 2}\left(\dfrac{C_\mu}{\mu_t}\right)^{1/2}(\rho\varepsilon)^{3/2} \end{bmatrix} \tag{43}$$

First, consider the k equation. Substitute the first expression in (43) into (9), we get

$$\delta U = U^1 - U^0 = \frac{\left[\dfrac{C_\mu}{\mu_t}\left(\mu_t P_k - \dfrac{C_\mu}{\mu_t}(\rho k)^2\right)^2\right](\Delta t)^3}{1 + 2\dfrac{C_\mu}{\mu_t}(\rho k)\Delta t + 2\left(\left(\dfrac{C_\mu}{\mu_t}\rho k\right)^2 - C_\mu P_k\right)(\Delta t)^2} \tag{44}$$

We just consider the limiting case of vanishing production term. In this case, we have

$$R = \frac{Y^3}{1 + 2Y + 2Y^2}$$

where

$$Y = \frac{C_\mu}{\mu_t}\rho k \cdot \Delta t = \frac{\varepsilon}{k}\Delta t$$

is the stiffness parameter. Obviously, R is an increasing function of Y. Hence, $(\varepsilon/k)\Delta t$ should be as small as possible.

Now, consider the ε equation. Substitute the second term in (43) into (9), we get

$$\delta U = U^1 - U^0 = \frac{\beta(\Delta t)^3 + \gamma(\Delta t)^4}{8 - \eta\Delta t - \theta(\Delta t)^2 - \xi(\Delta t)^3} \tag{45}$$

$$\beta = C_3^3 B^{-(1/2)} + C_3^2 C_4 B^{1/2} - 5C_3 C_4^2 B^{3/2} + 3C_4^3 B^{5/2} \tag{46}$$

$$\gamma = C_3^4 B^{-1} - 2C_3^3 C_4 + 2C_3 C_4^3 B^2 - C_4^4 B^2 \tag{47}$$

$$\eta = 4(C_3 B^{-(1/2)} - 3C_4 B^{1/2}) \tag{48}$$

$$\theta = 2(C_3^2 B^{-1} + 2C_3 C_4 - 3C_4^2 B) \tag{49}$$

$$\xi = \tfrac{1}{2}(3C_3^3 B^{-(3/2)} - 3C_3^3 C_4 B^{-(1/2)} - 3C_3 C_4^2 B^{1/2} + 3C_4^3 B^{3/2}) \tag{50}$$

where, $C_3 = C_{\varepsilon 1}(C_\mu \mu_t)^{1/2} P_k$, $C_4 = C_{\varepsilon 2}(\frac{C_\mu}{\mu_t})^{1/2}$ and $B = \rho\varepsilon$.

Now consider two limiting situations: vanishing production and vanishing dissipation.

Firstly, consider a vanishing production. From (45) we have, for

$$C_3 = C_{\varepsilon 1}(C_\mu \mu_t)^{1/2} P_k = 0$$

the following estimation:

$$R = \frac{\frac{3}{8}\left[\Delta t C_{\varepsilon 2}\left(\frac{C_\mu}{\mu_t}\rho\varepsilon\right)^{1/2}\right]^3 - \frac{1}{8}\left[\Delta t C_{\varepsilon 2}\left(\frac{C_\mu}{\mu_t}\rho\varepsilon\right)^{1/2}\right]^4}{1 + \frac{3}{2}\left[\Delta t C_{\varepsilon 2}\left(\frac{C_\mu}{\mu_t}\rho\varepsilon\right)^{1/2}\right] + \frac{3}{4}\left[\Delta t C_{\varepsilon 2}\left(\frac{C_\mu}{\mu_t}\rho\varepsilon\right)^{1/2}\right]^2 - \frac{3}{16}\left[\Delta t C_{\varepsilon 2}\left(\frac{C_\mu}{\mu_t}\rho\varepsilon\right)^{1/2}\right]^3}$$

$$= \frac{\frac{3}{8}Y^3 - \frac{1}{8}Y^4}{1 + \frac{3}{2}Y + \frac{3}{4}Y^2 - \frac{3}{16}Y^3} \tag{51}$$

where

$$Y = \Delta t C_{\varepsilon 2}\left(\frac{C\mu}{\mu_t}\right)^{1/2}(\rho\varepsilon)^{1/2} = C_{\varepsilon 2}\frac{\varepsilon}{k}\Delta t$$

In Figure 19 we display the error as a function of Y. It is clear that unless Y is very small, or strangely near 3, the error is very large. Hence, for the steady state error to be as small as possible, we require $(\varepsilon/k)\Delta t$ to be as small as possible, that is

$$\frac{\varepsilon}{k}\Delta t \to 0 \tag{52}$$

Now, consider a vanishing dissipation. The corresponding steady state error is given by

$$R = \frac{\frac{1}{8}Y^3 + \frac{1}{8}Y^4}{1 - \frac{1}{2}Y - \frac{1}{4}Y^2 - \frac{3}{16}Y^3} \tag{53}$$

where

$$Y = C_{\varepsilon 1} C_\mu P_k \left(\frac{k}{\varepsilon}\right)\Delta t \tag{54}$$

In Figure 20 we display the steady state error defined by (53). It is obvious that the steady state error can be small only if

$$\frac{k}{\varepsilon}\Delta t \to 0 \tag{55}$$

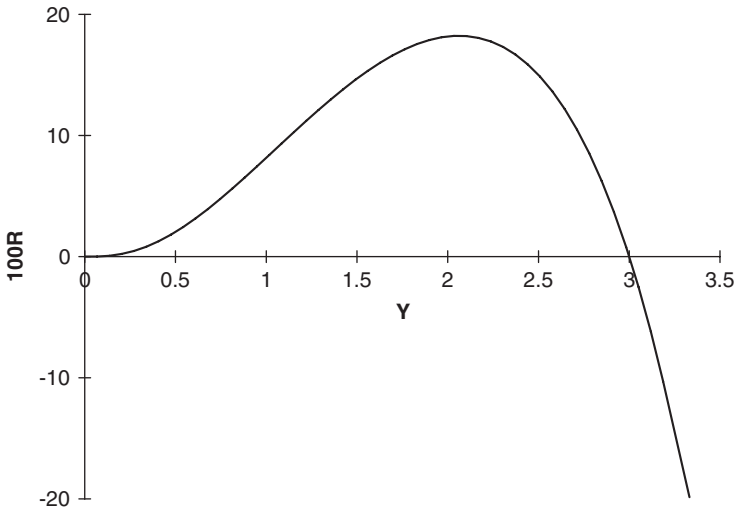

Figure 19. Steady state error for vanishing production term of the ε equation.

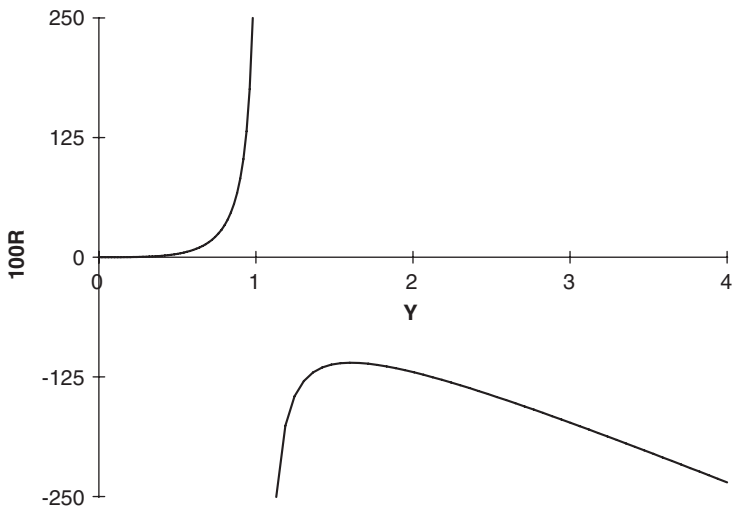

Figure 20. Steady state error of the ε equation for vanishing dissipation.

The two constraints (52) and (55) are entirely contradictory. Since the ratio k/ε could span all possible (positive) values in real computation, the time step will be required to be infinitely small for the steady state error to be small.

Hence, the time splitting method is nonconvergent for any finite values of the time step.

5. NUMERICAL RESULTS

In this section, we will give some numerical results with splitting method and unsplitting method for k–ε turbulent model. The governing equations are obtained by Favre-averaging the Navier–Stokes equations and modelling the Reynolds stress.

The Favre-averaged Navier–Stokes equations can be written as

$$\frac{\partial U}{\partial t}+\frac{\partial F_c}{\partial x}+\frac{\partial G_c}{\partial y}=\frac{\partial F_v}{\partial x}+\frac{\partial G_v}{\partial y} \tag{56}$$

with

$$U=\begin{pmatrix}\rho\\ \rho u\\ \rho v\\ \rho E\end{pmatrix},\quad F_c=\begin{pmatrix}\rho u\\ \rho u^2+p\\ \rho uv\\ (\rho E+p)u\end{pmatrix},\quad G_c=\begin{pmatrix}\rho v\\ \rho vu\\ \rho v^2+p\\ (\rho E+p)v\end{pmatrix} \tag{57}$$

Here, ρ, u, v, p and E denote the density, the x-wise velocity, the y -wise velocity, the static pressure and the total energy, respectively, and γ, with $\gamma=1.4$ for the present purposes is the ratio of specific heat. For a perfect gas, $p=(\gamma-1)\rho[E-\frac{1}{2}(u^2+v^2)-k]$, where we have included the turbulent kinetic energy k.

The viscous flux are defined by

$$F_v=\begin{pmatrix}0\\ \sigma_{xx}\\ \sigma_{xy}\\ u\sigma_{xx}+v\sigma_{xy}-q_x\end{pmatrix}\quad G_v=\begin{pmatrix}0\\ \sigma_{yx}\\ \sigma_{yy}\\ u\sigma_{yx}+v\sigma_{yy}-q_y\end{pmatrix} \tag{58}$$

where σ represents the stress tensor and q the heat flux vector, which are given by

$$\sigma_{xx}=2(\mu+\mu_t)\frac{\partial u}{\partial x}-\frac{2}{3}(\mu+\mu_t)\left(\frac{\partial u}{\partial x}+\frac{\partial v}{\partial y}\right)-\frac{2}{3}\rho k \tag{59}$$

$$\sigma_{yy}=2(\mu+\mu_t)\frac{\partial v}{\partial y}-\frac{2}{3}(\mu+\mu_t)\left(\frac{\partial u}{\partial x}+\frac{\partial v}{\partial y}\right)-\frac{2}{3}\rho k \tag{60}$$

$$\sigma_{xy}=\sigma_{yx}=(\mu+\mu_t)\left(\frac{\partial u}{\partial x}+\frac{\partial v}{\partial y}\right) \tag{61}$$

$$q_x=-\frac{\gamma}{\gamma-1}\left(\frac{\mu}{Pr}+\frac{\mu_t}{Pr_t}\right)\frac{\partial(p/\rho)}{\partial x} \tag{62}$$

$$q_y=-\frac{\gamma}{\gamma-1}\left(\frac{\mu}{Pr}+\frac{\mu_t}{Pr_t}\right)\frac{\partial(p/\rho)}{\partial y} \tag{63}$$

Here, Pr is the laminar Prandtl number, which is taken as 0.7 for air, Pr_t is the turbulent Prandtl number, taken as 0.9. The molecule dynamic viscosity μ is assumed to be a function of the temperature, following the well-known Sutherland's law.

$$\mu = \mu_{273}\left(\frac{T}{273}\right)^{3/2}\frac{273+T_0}{T+T_0} \tag{64}$$

where $\mu_{273} = 17.1\,\mu\text{Pa s}$, $T_0 = 110\,\text{K}$. The Stokes hypothesis ($\lambda = -2\mu/3$) is adopted.

The convective numerical flux at the cell interface is evaluated using Roe's approximate Riemann solver [23]

$$F_{i+(1/2),j} = \tfrac{1}{2}[F_c(U^{\text{L}}) + F_c(U^{\text{R}})] - \tfrac{1}{2}|A_{\text{Roe}}|(U^{\text{R}} - U^{\text{L}}) \tag{65}$$

where U^{L} and U^{R} are the left- and right-hand states of the solution at the interface, constructed using the MUSCL method [24] to attain higher order accuracy, and A_{Roe} is the well-known Roe matrix. This means that we use a linear approximation of the solution on each cell to calculate the interface values, rather than a piecewise constant solution. The MUSCL scheme is implemented as

$$U^{\text{L}} = U_{i,j} + \left\{\left(\frac{s}{4}\right)[(1-\kappa s)\Delta_- + (1+\kappa s)\Delta_+]U\right\}_{i,j} \tag{66}$$

$$U^{\text{R}} = U_{i,j} - \left\{\left(\frac{s}{4}\right)[(1+\kappa s)\Delta_- + (1-\kappa s)\Delta_+]U\right\}_{i,j} \tag{67}$$

where, Δ_- and Δ_+ are the forward and backward difference operators, respectively. The parameter, κ, determines the spatial accuracy of the interpolation. Here, $\kappa = +\frac{1}{3}$ is chosen for a third-order upwind biased scheme. Limiters may be used in order to eliminate spurious wiggles at discontinuities [25]. In this paper, we have introduced a slope limiter, s, as given below.

$$s = \frac{2\Delta_+\Delta_- + \vartheta}{(\Delta_+)^2 + (\Delta_-)^2 + \vartheta} \tag{68}$$

Here, ϑ is used to avoid denominator to be zero, which is chosen 10^{-6}.

Let $R(U^n)$ represent the contribution from the space discretization of the Favre-averaged Navier–Stokes equations plus the turbulence models. To advance the solution in time, we use a simplified four-stage Runge–Kutta scheme [26] as defined by

$$\begin{aligned} U^{(0)} &= U^n \\ U^{(i)} &= U^{(0)} + \alpha_i \Delta t R(U^{(i-1)}), \quad i = 1,\ldots,4 \\ U^{n+1} &= U^{(4)} \end{aligned} \tag{69}$$

with $\{\alpha_1, \alpha_2, \alpha_3, \alpha_4\} = \{\frac{1}{4}, \frac{1}{3}, \frac{1}{2}, 1\}$.

Table I. The closure coefficients for turbulence model.

Model	$\mathbf{C}_{\varepsilon 1}$	$\mathbf{C}_{\varepsilon 2}$	C_μ	σ_k	σ_ε
JL	1.55	2.00	0.09	1.0	1.3
LS	1.44	1.92	0.09	1.0	1.3
LB	1.44	1.92	0.09	1.0	1.3
HL	1.44	1.92	0.09	$1.4-1.1\mathrm{e}^{-(y_\lambda/10)}$	$1.3-1.0\mathrm{e}^{-(y_\lambda/10)}$

The time step is determined by

$$\Delta t = \frac{\mathrm{CFL}}{|\nabla\xi|\,t_1 + |\nabla\eta|\,t_2}$$
$$t_1 = |\bar{U}| + a + 2|\nabla\xi|(\mu+\mu_T)\max\left(\frac{4}{3},\frac{\gamma}{Pr}\right)\frac{Ma}{Re}\frac{1}{\rho} \tag{70}$$
$$t_2 = |\bar{V}| + a + 2|\nabla\eta|(\mu+\mu_T)\max\left(\frac{4}{3},\frac{\gamma}{Pr}\right)\frac{Ma}{Re}\frac{1}{\rho}$$

For the scheme to be stable, CFL is usually bounded from a value of order of unity. Local time stepping and implicit residual smoothing [26] are used to accelerate computation.

We solve plane jet flow problem with Navier–Stokes equations coupled with standard k–ε turbulent model, and solve the other flow problem with Navier–Stokes equations coupled with low-Reynolds k–ε turbulent models. These low-Reynolds k–ε turbulent models include (1) Jones–Launder model (JL) [6], (2) the Launder–Sharma model (LS) [27], (3) the Lam–Bremhorst model (LB) [28], and (4) the Hwang–Lin model (HL) [29] low-Reynolds k–ε turbulent model.

Model 2 is actually extensions of the JL model, which have been introduced to improve some of the drawbacks of the standard k–ε model, mainly being the numerical stiffness associated with the source terms. The HL model is based on the near-wall characteristic obtained with direct numerical simulation data. Let $y_\lambda = \frac{y}{\sqrt{\nu k/\tilde{\varepsilon}}}$, $R_t \equiv \frac{k^2}{(\nu\tilde{\varepsilon})}$, $R_y = \frac{\sqrt{k}y}{\nu}$, $S = \sqrt{2S_{i,j}S_{i,j}}$, $S_{i,j} = (U_{i,j} + U_{i,i})/2$. The damping functions appearing in the source term (38) are summarized in Tables I–III.

5.1. Plane jet flow

This problem has been studied experimentally in Reference [30]. The corresponding Reynolds number is 3×10^4 and Mach number is $M_\infty = 0.6$. The initial mean velocity profile is defined as

$$u = \exp(-81\eta^2), \quad \eta = \frac{y}{x+1} \tag{71}$$

The splitting method diverges, while the unsplit method converges. The convergence histories are shown in Figure 21. The spreading rate is shown in Figure 22.

Table II. The damping function for various models I.

Model	$\mathbf{f}_1$	$\mathbf{f}_2$	T_l	f_μ
JL	1	$1-0.3\mathrm{e}^{-Re_t^2}$	$\frac{k}{\tilde{\varepsilon}}$	$\mathrm{e}^{-[2.5/(1+\frac{Re_T}{50})^2]}$
LS	1	$1-0.3\mathrm{e}^{-Re_t^2}$	$\frac{k}{\tilde{\varepsilon}}$	$\mathrm{e}^{-[3.4/(1+\frac{Re_T}{50})^2]}$
LB	$1+\left(\frac{0.05}{f_\mu}\right)^3$	$1-\mathrm{e}^{-Re_t^2}$	$\frac{k}{\tilde{\varepsilon}}$	$\frac{(1-\mathrm{e}^{-0.0165R_y})^2}{\left(1+\frac{20.5}{Re_T}\right)^{-1}}$
HL	1	1	$\frac{k}{\tilde{\varepsilon}}$	$1-\mathrm{e}^{-0.01y_\lambda^*-0.008y_\lambda^{*3}}$

Table III. The damping function for various models II.

Model	D	E_k	E_ε
JL	$2\nu\left(\frac{\partial\sqrt{k}}{\partial n}\right)^2$	$2\nu\left(\frac{\partial\sqrt{k}}{\partial x_k}\right)^2$	$2\nu\nu_T\left(\frac{\partial^2 U}{\partial x_k\partial x_l}\right)^2$
LS	$2\nu\left(\frac{\partial\sqrt{k}}{\partial n}\right)^2$	$2\nu\left(\frac{\partial\sqrt{k}}{\partial x_k}\right)^2$	$2\nu\nu_T\left(\frac{\partial^2 U}{\partial x_k\partial x_l}\right)^2$
LB	0	0	0
HL	$2\nu\left(\frac{\partial\sqrt{k}}{\partial n}\right)^2$	$2\nu\left(\frac{\partial\sqrt{k}}{\partial x_k}\right)^2-\frac{1}{2}\frac{\partial}{\partial x_j}(\nu\frac{k}{\varepsilon}\frac{\partial D}{\partial x_j})$	$-\frac{1}{2}\frac{\partial}{\partial x_j}(\nu\frac{\tilde{\varepsilon}}{k}\frac{\partial k}{\partial x_j})$

5.2. *Flat plane flow*

Flow with a zero-pressure gradient was calculated over a flat plate. Inflow Mach is 0.2, and Reynolds number is 6×10^6. A Cartesian mesh with 65 points in the axial direction and 97 points normal to the viscous wall is used to model this flow. The first 16 grid points upstream of the leading edge of the flat plate are treated as an inviscid wall to provide a uniform profile at the leading edge location. The value of y^+ for the first layer grid near the wall is no more than 0.25.

The error L_2 is defined by

$$L_2=\sqrt{\frac{\sum_j|R(U_j^n)|^2}{N_{\text{Total}}}} \tag{72}$$

where N_{Total} is the total grid number and $R(U_j^n)$ is the space residual.

The convergence history with splitting and unsplit mixed method for four different turbulent models, respectively, are displayed in Figures 23–26. At the same time steps, the solution is stable with the method based on unsplitting, while unstable with the method based on splitting method. Figure 27 shows the velocity profile of flat plane at $x=0.8$. Figure 28 shows the skin friction.

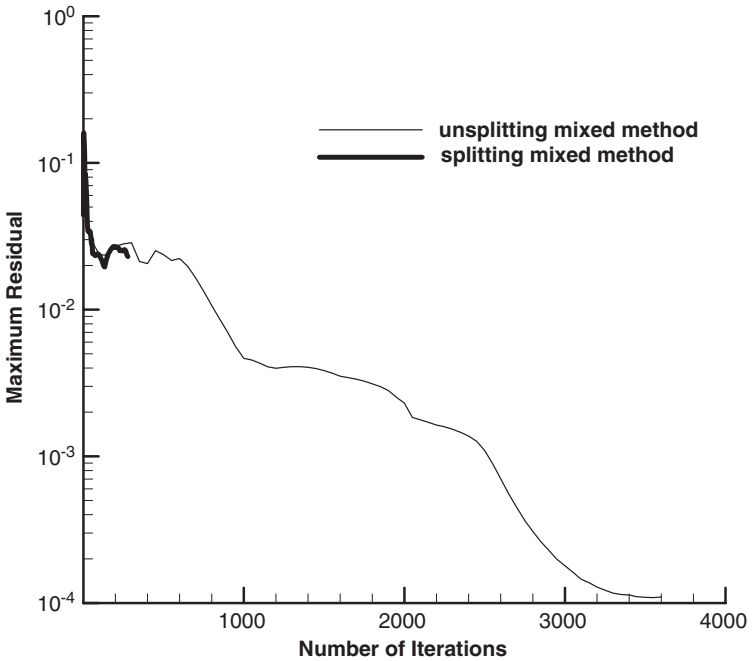

Figure 21. The convergence histories for turbulent jet flow.

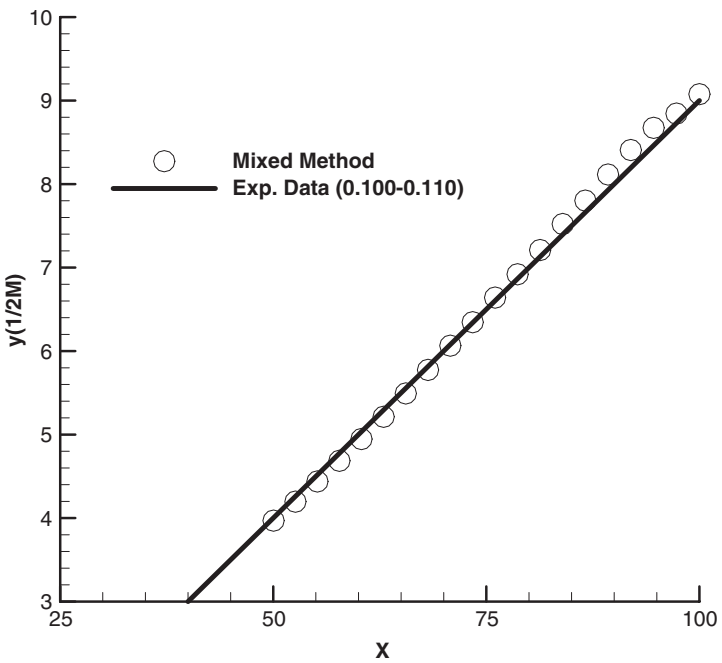

Figure 22. Spreading rate for plane jet flow. The numerical solution is obtained by the mixed method.

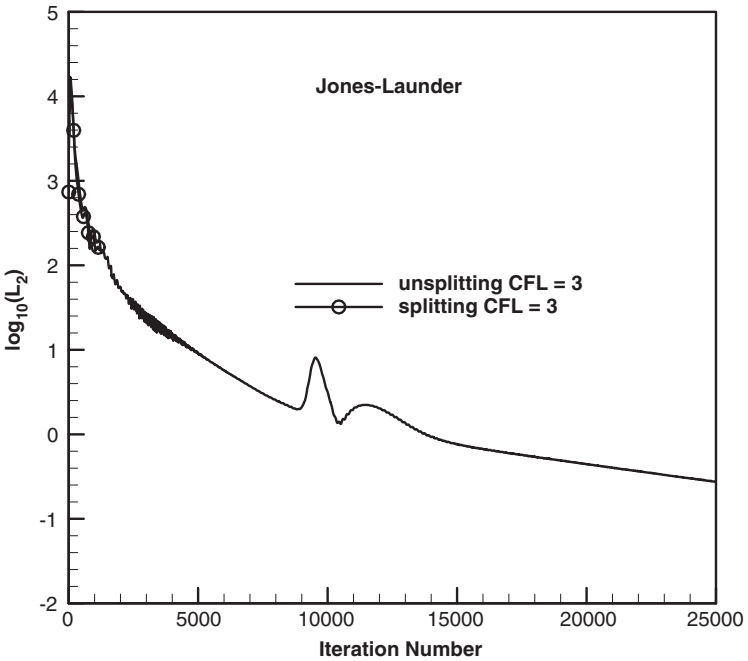

Figure 23. The convergence history for flat plane (JL model).

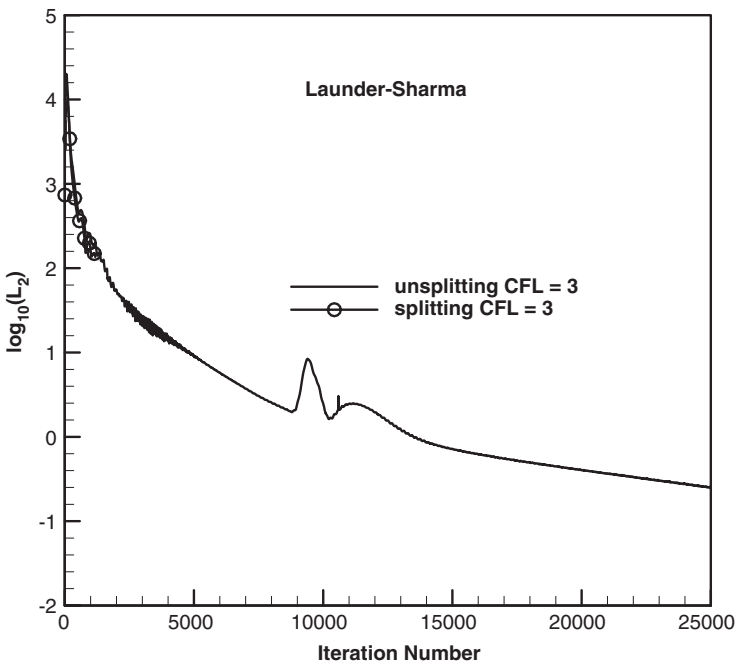

Figure 24. The convergence history for flat plane (LS model).

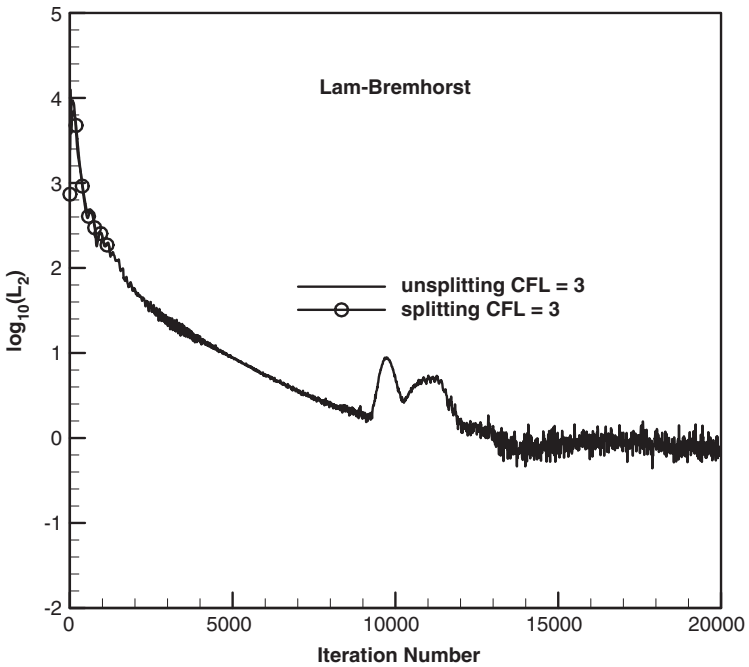

Figure 25. The convergence history for flat plane (LB model).

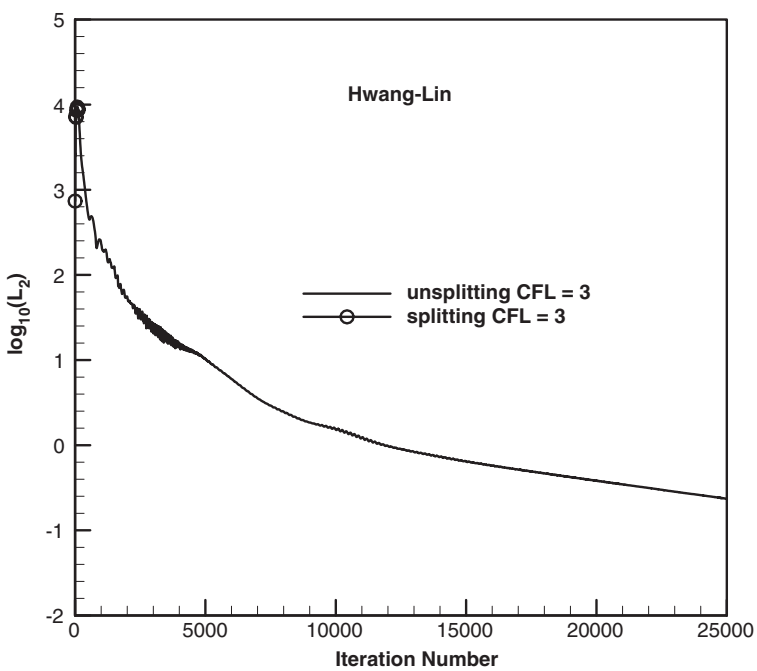

Figure 26. The convergence history for flat plane (HL model).

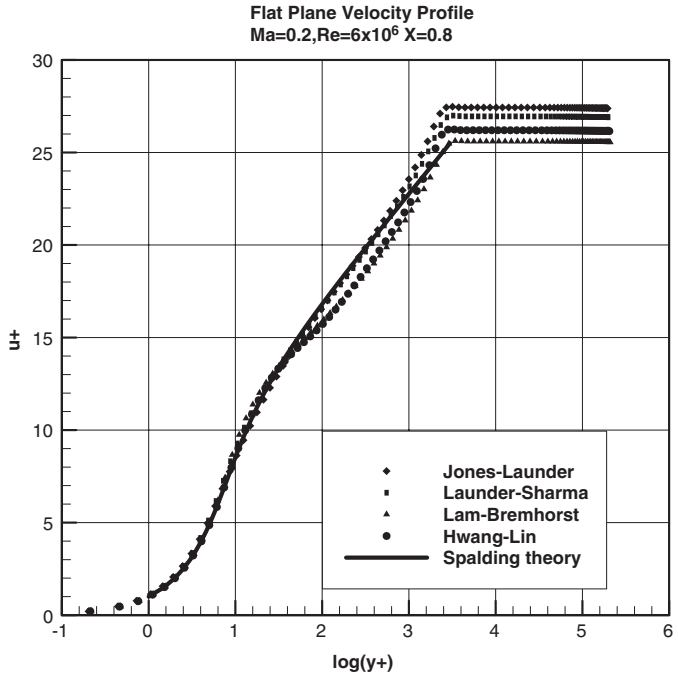

Figure 27. The flat plane velocity profile (position $x = 0.8$).

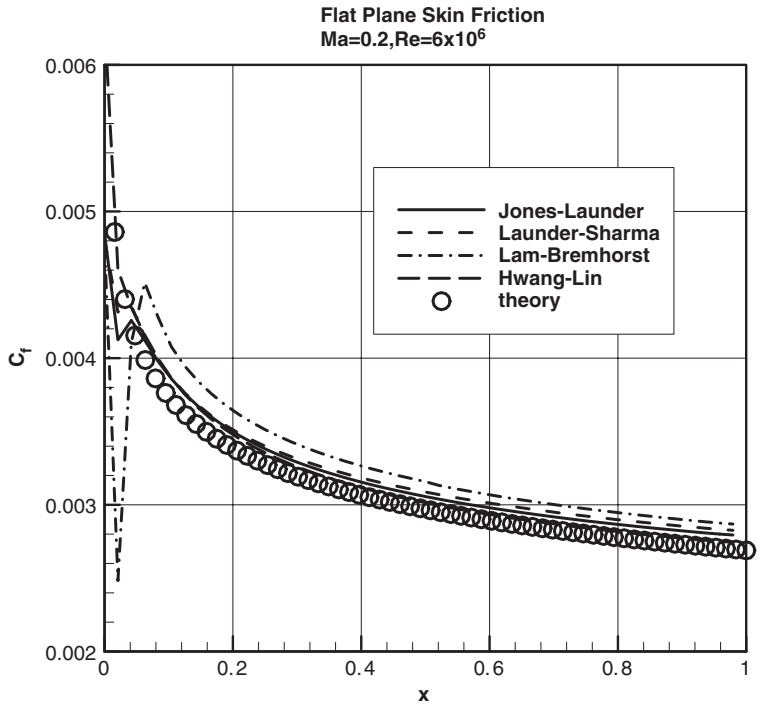

Figure 28. The flat plane skin friction.

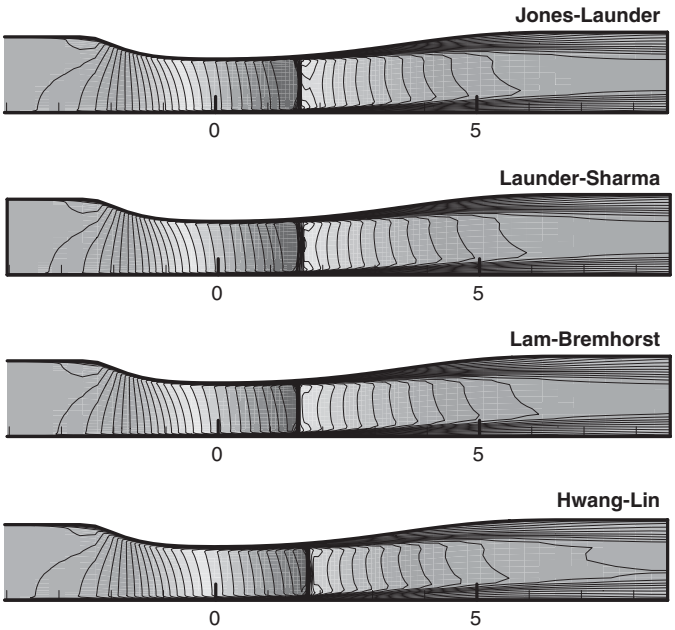

Figure 29. The Mach contour of transonic diffuser for $R = 0.82$ (weak shock).

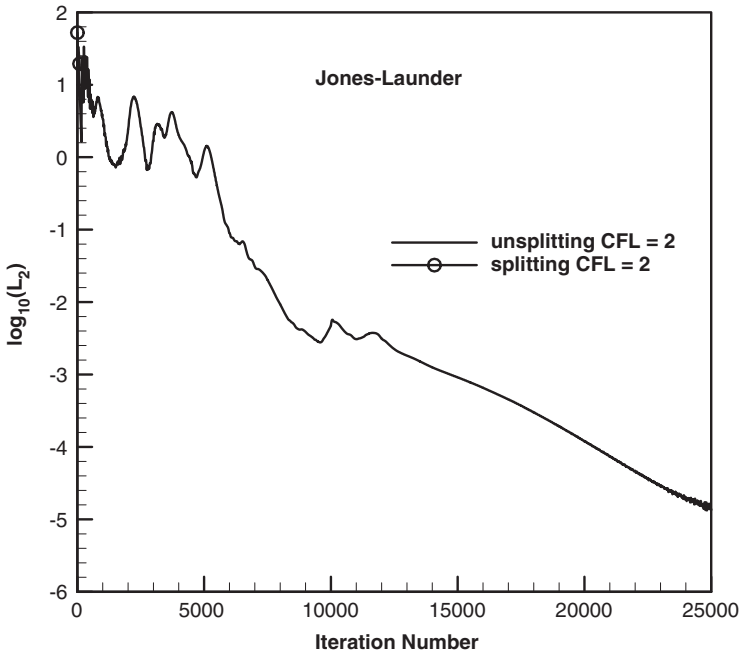

Figure 30. The convergence history for transonic diffuser (JL model): mixed method.

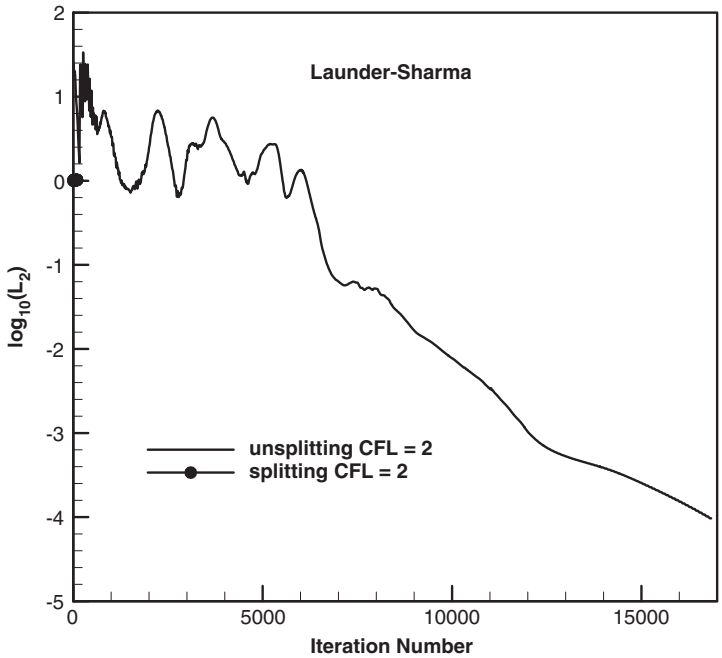

Figure 31. The convergence history for transonic diffuser (LS model): mixed method.

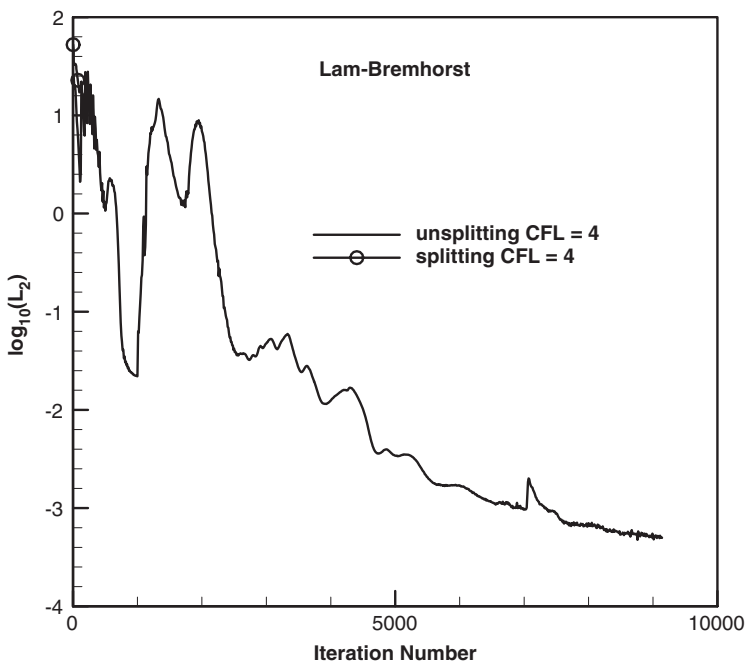

Figure 32. The convergence history for transonic diffuser (LB model): mixed method.

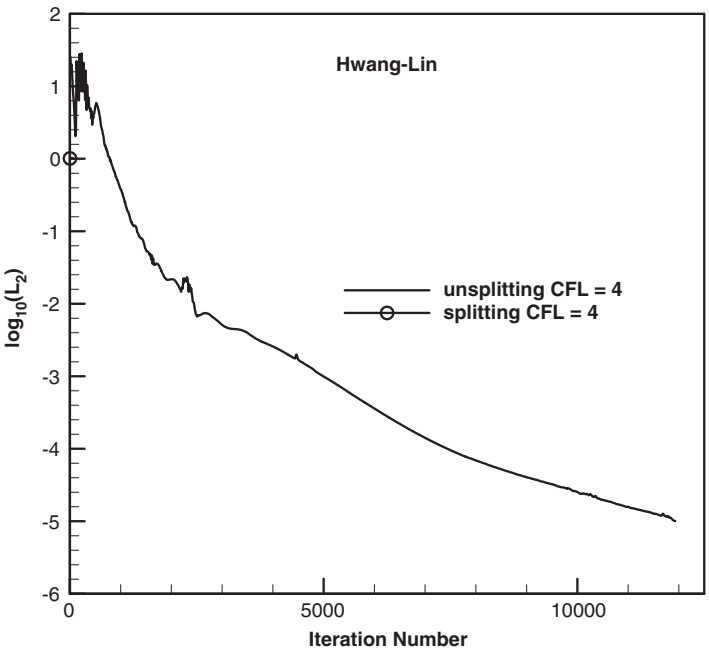

Figure 33. The convergence history for transonic diffuser (HL model): mixed method.

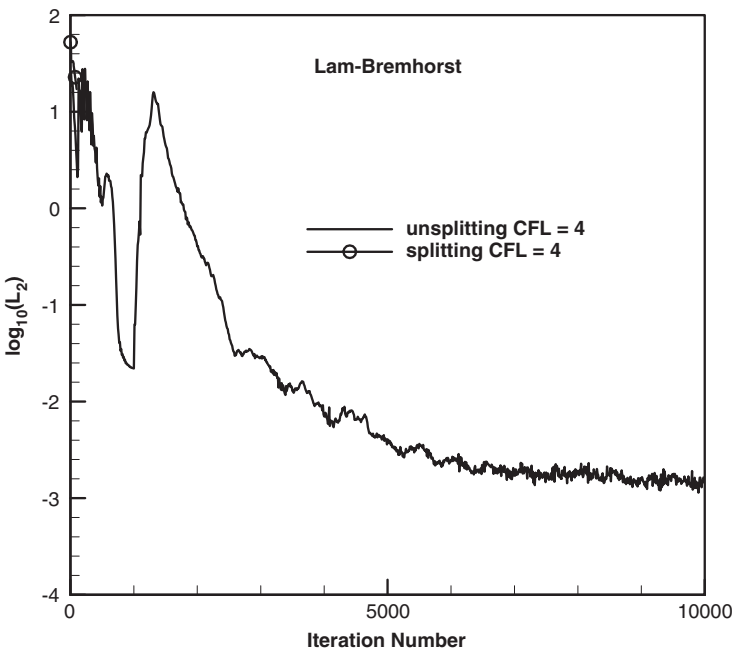

Figure 34. The convergence history for transonic diffuser (LB model): conventional method.

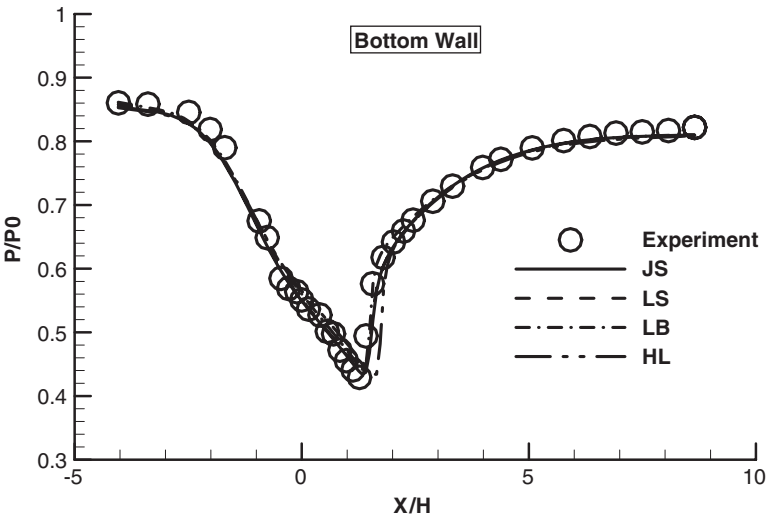

Figure 35. The static pressure distribution along bottom wall.

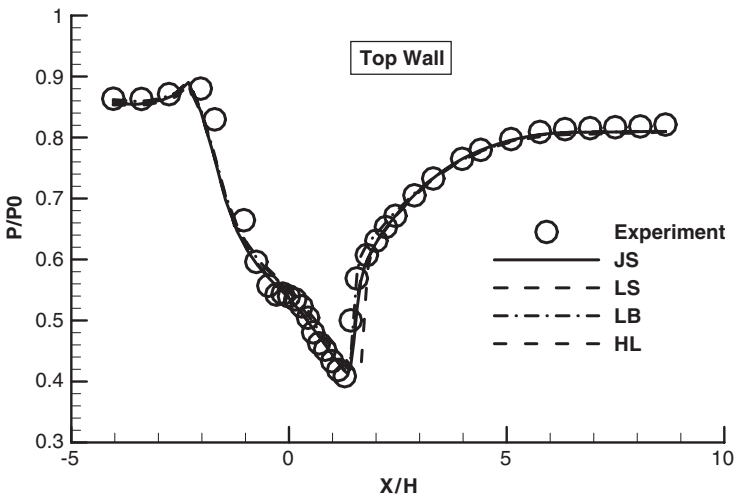

Figure 36. The static pressure distribution along top wall.

5.3. Transonic diffuser

We consider transonic flow with a weak shock through a converging diverging diffuser. The experiment has been carried out by Sajben and Kroutil [31]. This configuration has an entrance to throat area ratio of 1.4, an exit to throat area ratio of 1.5, and a sidewall spacing of approximately four throat heights. Varying the exit pressure leads to different shock positions and strengths. The corresponding Reynolds number is 9.370×10^5 and the Mach number is

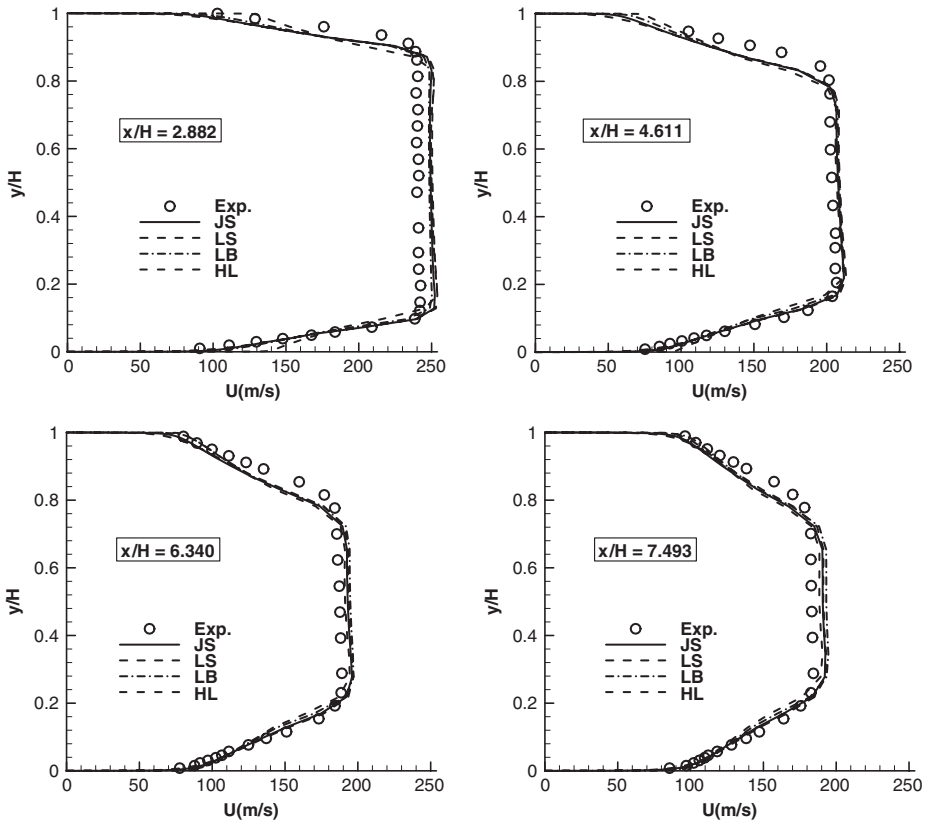

Figure 37. Velocity profiles at four axial locations for the Sajben diffuser. Numerical results are obtained with the mixed method.

$Ma = 0.9$. The total pressure at inflow is 1.349×10^5 Pa, the static pressure at the outflow is 1.11×10^5 Pa.

The convergence history with mixed method for various turbulent models is shown in Figures 30–33. We see the computation based on splitting method fails to converge, while all models with unsplitting method converge. All computations based on splitting time are unstable. If we adopt the traditional method based on splitting method to solve the k–ε turbulence model, the computation is also unstable. Here, we only give one example in Figure 34. In this figure, unsplitting method converge, while splitting method is still unstable for Lam–Bremhorst turbulence model computation. The computation also shows that the mixed method can weaken the restriction of the time step size for source term, implicit residual smoothing can increase the CFL number by a factor of 4, and get convergence at larger time step.

The Mach contour with mixed method for various turbulent models is shown in Figure 29. The static pressure distribution along the bottom and top walls are shown in Figures 35 and 36, respectively, in comparison with the experimentally measured values. Figure 37 displays the velocity profiles at four axial locations, $x/H = 2.882$, 4.611, 6.340 and 7.493, downstream of the shock wave. The agreement between computation and experiment is good. Figures 38 and 39

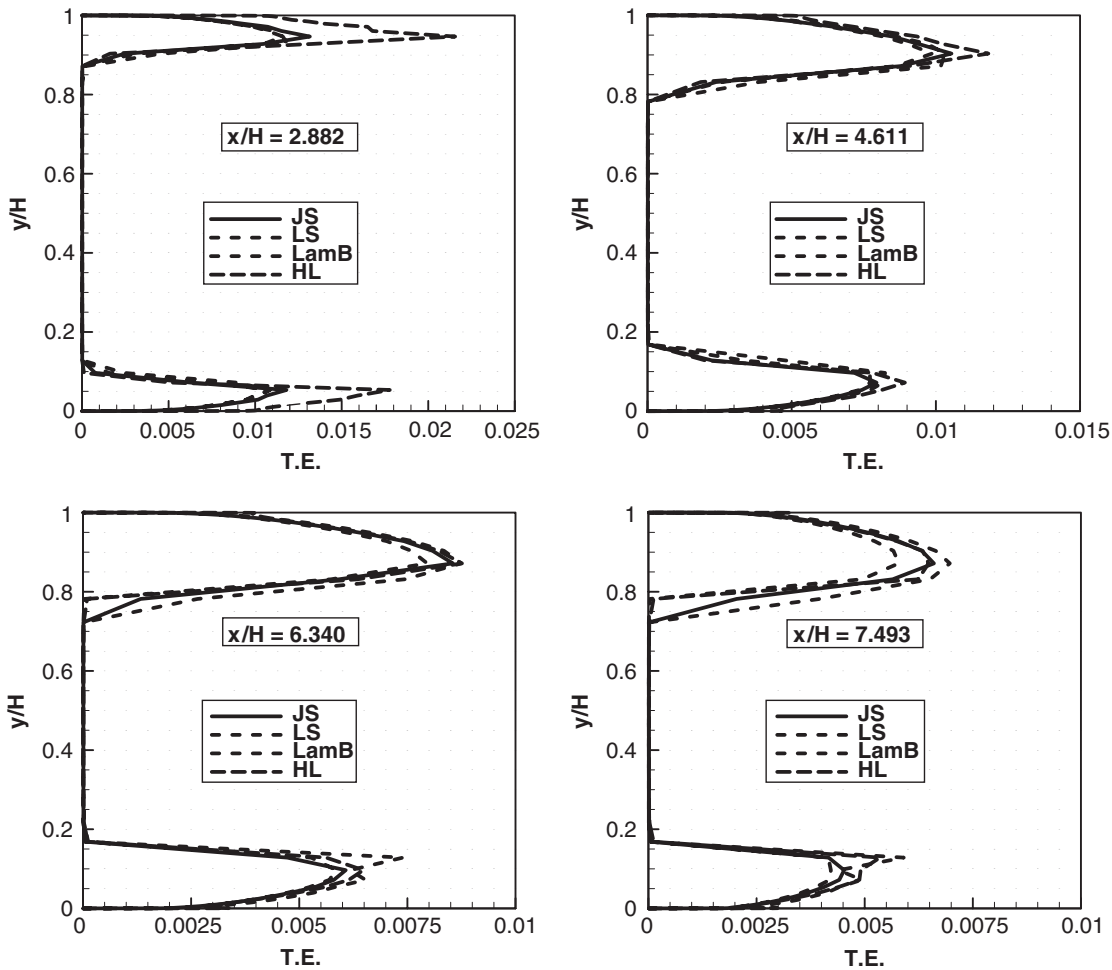

Figure 38. Turbulent kinetic energy k profiles at four axial locations for the Sajben diffuser.

display the turbulent kinetic energy k and turbulent dissipation rate ε profiles, respectively, at four different axial locations. Sharp gradients of the turbulent quantities are mainly confined to the near-wall regions.

6. CONCLUDING REMARKS

We have analysed the convergence to a steady state for the time splitting method approximating the k–ε turbulence models. This analysis is based on a proper definition of the steady state error, which is the departure of the numerical solution from the steady state solution. Comparisons between analysis and numerical computations for a scalar equation with various source terms support the validity of the analysis. We have, therefore, applied this analysis

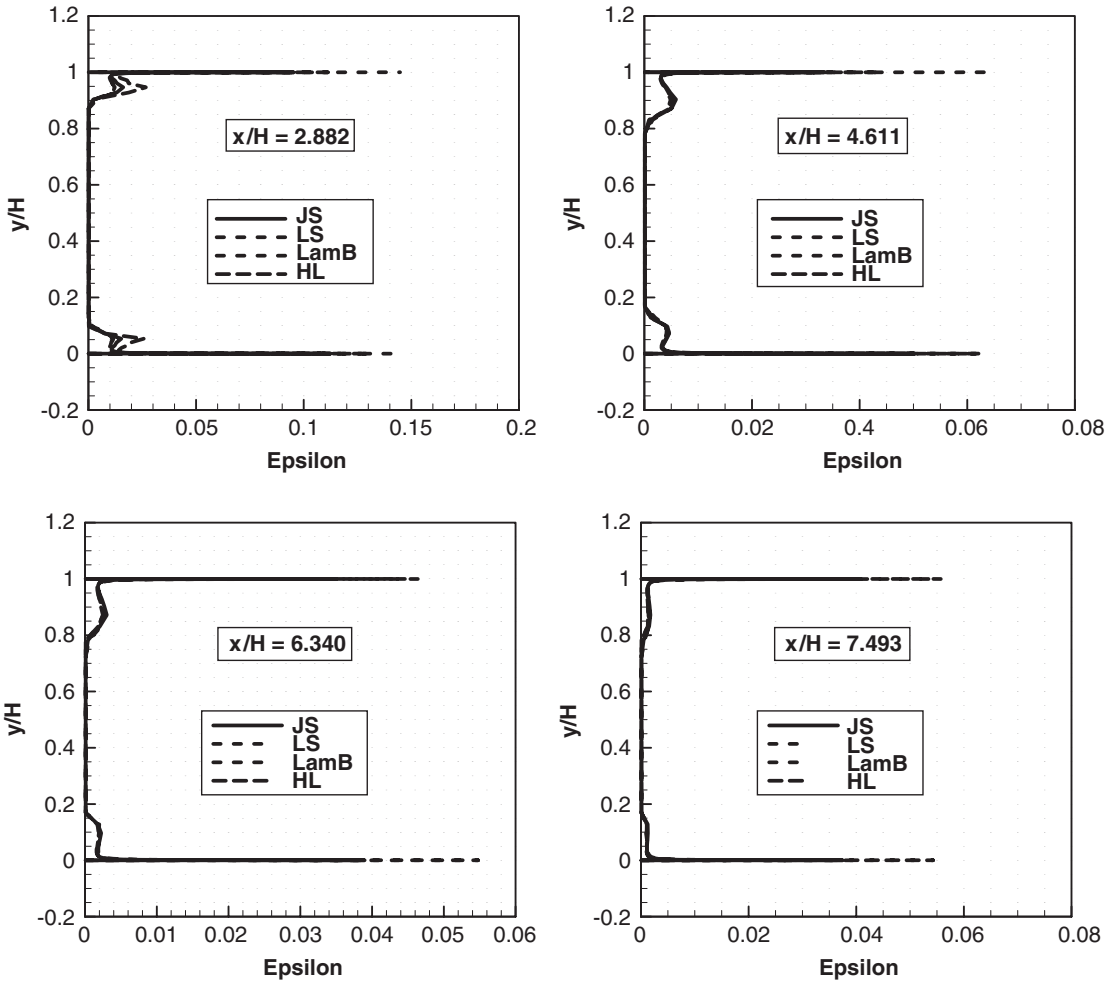

Figure 39. Turbulent dissipation rate ε profiles at four axial locations for the Sajben diffuser.

to the case of k–ε turbulence models, and found that the time splitting method is always nonconvergent. Numerical experiments for various kinds of turbulence flows confirm that the time splitting method is always nonconvergent, while the unsplit method could be convergent.

In the future we will attempt to extend the unsplitting mixed analytical/numerical method to three-dimensional turbulent flow computations.

REFERENCES

1. Du T, Shi J, Wu ZN. Mixed analytical/numerical method for flow equations with a source term. *Computers and Fluids* 2003; **32**(5):659–690.
2. Du T, Wu ZN. Mixed analytical/numerical method applied to the high Reynolds number k–ε turbulence model. *Computers and Fluids* 2005; **34**(1):97–119.

3. Du T, Wu ZN. Mixed analytical/numerical method for low Reynolds number turbulence model. *AIAA Journal* 2004; **42**:1140–1153.
4. Huang PG, Coakley TJ. An implicit Navier–Stokes code for turbulent flow modeling. *AIAA 30th Aerospace Sciences Meeting*, Reno, NV, *AIAA Paper 92-0547*.
5. Merci B, Steelant J *et al*. Computational treatment of source terms in two-equation turbulence models. *AIAA Journal* 2000; **38**(11):2085–2093.
6. Jones WP, Launder BE. The calculation of low-Reynolds-number phenomena with a two-equation model of turbulence. *International Journal of Heat and Mass Transfer* 1974; **16**:1119–1130.
7. Sahu J, Danberg JE. Navier–Stokes computations of transonic flows with a two-equation turbulence model. *AIAA Journal* 1991; **24**:1744–1751.
8. Zhao Y. Stable computation of turbulent flow with a low-Reynolds-number K–ε turbulence model and explicit solver. *Advances in Engineering Software* 1997; **28**:487–499.
9. Toro EF. *Riemann Solvers and Numerical Methods for Fluid Dynamics*: *A Practical Introduction*. Springer: Berlin, 1999.
10. Kruzkov SN. First order quasi-linear equation in several independent variables. *Mathematics of the USSR-Sbornik* 1970; **10**:217–243.
11. Monthé LA. A study of splitting scheme for hyperbolic conservation laws with source terms. *Journal of Computational and Applied Mathematics* 2001; **137**:1–12.
12. Tang T, Teng Z-H. Error bounds for fractional step methods for conservation laws with source terms. *SIAM Journal on Numerical Analysis* 1995; **32**:110–127.
13. Gosse L. A well-balanced scheme using non-conservative products designed for hyperbolic systems of conservation laws with source terms. *Mathematical Models and Methods in Applied Sciences* 2001; **11**:339–365.
14. Greenberg JM, Le Roux A-Y. A well-balanced scheme for the numerical processing of source terms in hyperbolic equations. *SIAM Journal on Numerical Analysis* 1996; **33**:1–16.
15. LeVeque RJ. Balancing source terms and flux and flux gradients in high-resolution Godunov methods: the quasi-steady wave-propagation algorithm. *Journal of Computational Physics* 1998; **146**:346–365.
16. Strang G. On the construction and comparison of difference schemes. *SIAM Journal on Numerical Analysis* 1968; **5**:506–517.
17. Yanenko NN. *The Method of Fractional Steps*. Springer: New York, 1971.
18. Hairer E, Lubich C, Wanner G. *Geometric Numerical Integration*. Springer Series in Computational Mathematics, vol. 31. Springer: Berlin, 2002.
19. McLachlan RI, Quispel GRW. Splitting methods. *Acta Numerica* 2002; **11**:341–434.
20. Roman K, Anne K, Brynjulf O. The behaviour of the local error in splitting methods applied to stiff problems. *Journal of Computational Physics* 2004; **195**:576–593.
21. LeVeque RJ, Yee HC. A study of numerical methods for hyperbolic conservation laws with stiff source terms. *Journal of Computational Physics* 1990; **86**:187–210.
22. Yee HC. Construction of explicit and implicit symmetric TVD schemes and their applications. *Journal of Computational Physics* 1987; **68**:151–179.
23. Roe PL. Approximate Riemann solvers, parameter vectors, and difference schemes. *Journal of Computational Physics* 1981; **43**:357–372.
24. van Leer B. Towards the ultimate conservative difference scheme. V. A second-order sequel to Godunov's method. *Journal of Computational Physics* 1979; **32**:101–136.
25. Anderson WK, Thomas JL, van Leer B. Comparison of finite volume flux vector splitting for the Euler equations. *AIAA Journal* 1986; **24**:1453–1460.
26. Jameson A, Baker TJ. Solution of the Euler equations for complex configurations. *AIAA-Paper 83-1929*, 1983.
27. Launder BE, Sharma BI. Application of the energy dissipation model of turbulence to the calculation of flow near a spinning disc. *Letters in Heat and Mass Transfer* 1974; **1**(2):131–138.
28. Lam CKG, Bremhorst KA. A modified form of the k–ε model for predicting wall turbulence. *ASME Journal of Fluids Engineering* 1981; **103**:456–459.
29. Hwang CB, Lin CA. Improved low-Reynolds-number model based on direct numerical simulation data. *AIAA Journal* 1998; **36**(1):38–43.
30. Bradbury LJS. The structure of a self-preserving turbulent plane jet. *Journal of Fluid Mechanics* 1965; **23**:31–64.
31. Sajben M, Kroutil JC. Effects of initial boundary-layer thickness on transonic diffuser flows. *AIAA Journal* 1981; **19**(11):1386–1393.

